Electronic Supplementary Information

Host–Guest Binding Between Cucurbit[8]uril and Amphiphilic Peptide Achieved Tunable Supramolecular Aggregates for Cancer Diagnosis

Jie Niu,[a] Jie Yu,[a] Xuan Wu,[c] Ying-Ming Zhang,[a] Yong Chen,[a] Zhilin Yu[b] and Yu Liu[a*]*

[a] College of Chemistry, State Key Laboratory of Elemento-Organic Chemistry, Nankai University, Tianjin 300071, P. R. China, Collaborative Innovation Center of Chemical Science and Engineering, Tianjin 300071, P. R. China
[b] Key Laboratory of Functional Polymer Materials, Ministry of Education, State Key Laboratory of Medicinal Chemical Biology, Institute of Polymer Chemistry, College of Chemistry, Nankai University, Tianjin 300071, China
[c] School of Chemistry and Chemical Engineering, Yangzhou University, Yangzhou, Jiangsu 225002, P. R. China
*E-mail: ymzhang@nankai.edu.cn; yuliu@nankai.edu.cn

Contents

1. General information 3
2. Synthesis and characterization of target molecules 5
3. ^{1}H NMR of peptides and CB[8] 11
4. ITC spectra of peptides and CB[8] 13
5. Electrostatic potential surfaces of peptides 14
6. Characterization of M^{O}LGG-6C 15
7. Electrostatic potential surfaces of MLGG-6C and M^{O}LGG-6C 17
8. UV-Vis titration, ITC titration and fluorescence spectra of CB[8] and PDI 18
9. 2D DOSY NMR spectra of CB[8] and PDI 20
10. Fluorescence spectra spectra of CB[7] and PD 21
11. Fluorescence spectra for adding MLGG-6C to PDI⊂CB[8] and PDI 22
12. UV-Vis absorbance, and ITC titration spectra for adding MLGG-6C to PDI⊂CB[8] 23
13. Stability test of PDI 24
14. Quantum yield spectra of PDI 25
15. Fluorescence lifetime spectra of PDI 27
16. Oxidation properties of YLGGG and CLGGG peptides 29
17. TEM images of MLGG and PDI with CB[8] 34
18. TEM images of PDI/MLGG-6C⊂CB[8] at different pH 36
19. Fluorescence and TEM of PDI/MLGG-6C⊂CB[8] assembly 37

20.ROS CLSM images of PDI/MLGG-6C⊂CB[8] assembly 38
21. CLSM images of PDI/MLGG-6C⊂CB[8] assembly 39
22. Pearson correlation coefficient of PDI/MLGG-6C⊂CB[8] assembly 40
23. Cell viability of MLGG-6C and MLGG-6C⊂CB[8] 41
24. ROS CLSM images and cell viability at elevated ROS level 42
25. ROS CLSM images and cell viability in normal cells 43
References 44

1. General information

Materials. All reagents and solvents were obtained from commercial suppliers and used as received unless specified otherwise. All aqueous solutions were prepared with distilled water. MLGG-6C, MLGGG, M^{O}LGGG, M^{O2}LGGG, LMGGG, LM^{O}GGG, LM^{O2}GGG and the reference compounds YLGGG and CLGGG were synthesized by the Nanjing Genscript Co., Ltd.

Instrumentation and methods ^{1}H NMR spectra were recorded on a Bruker DMX 400 MHz spectrometer. High-resolution mass spectrum was recorded on Varian 7.0 T FTMS with the MALDI ion source. TEM images were obtained on a Tecnai G2F20 microscope (FEI) at an accelerating voltage of 200 kV. SEM images were obtained on ZEISS MERLIN Compact. AFM images were obtained on Bruker Dimension Icon. The samples were prepared by placing a drop of solution onto a carbon-coated copper grid, silicon pellet, mica plate, respectively, and air-drying it. UV-Vis spectra were recorded in a quartz cell (light path = 1 cm) on a Shimadzu UV-3600 spectrophotometer equipped with a PTC-348WI temperature controller. DLSs were measured by Brookhaven instrument. The fluorescent confocal images (LSCM) were carried out on an Olympus FV1000 fluorescence microscope. The biological electron microscope images were obtained on HITACHI HT7700 Exalens and the samples were prepared by Wuhan Servicebio Co., Ltd.

Preparation of MLGG-6C⊂CB[8] assembly: The solution of CB[8] and MLGG-6C was mixed and sonicated for 30 min and then gave the binary the nanoparticles.

Non-linear fitting equation: The formula for nonlinear fitting is according to the literature[S1]

$$\Delta A_{obs} = \varepsilon_{\Delta HG} \times \left(\frac{1}{2} \times \left([G]_0 + [H]_0 + \frac{1}{K_a}\right) - \sqrt{([G]_0 + [H]_0 + \frac{1}{K_a})^2 + 4 \times [H]_0 \times [G]_0}\right)$$

where ΔA_{obs} is the UV-vis absorbance change of **G** at [H], $\varepsilon_{\Delta HG}$ is molar adsorption coefficient of **G** when the guest is completely complexed; $[G]_0$ is the fixed initial concentration of the guest; and [H] is the varying concentrations of the host.

Isothermal Titration Calorimetry (ITC). A thermostated and fully computer-operated isothermal calorimetry instrument was used for all the microcalorimetric experiments. The ITC experiments were performed at 25 °C in phosphate buffer solution (pH 7.3, 10 mM), giving the stability constants (K_S) and the thermodynamic parameters (ΔH and ΔS) upon complexation. In each run, a solution of peptides in a 0.250 mL syringe was sequentially injected with stirring at 300 rpm into a solution of CB[8] host in the sample cell (1.4227 mL volume). A control experiment to determine the heat of dilution was carried out for each run by performing the same number of injections with the same concentration of guest compound as used in the titration experiments into a same solution in the

absence of host compound. The dilution enthalpies determined in control experiments were subtracted from the enthalpies measured in the titration experiments to obtain the net reaction heat. All thermodynamic parameters reported in this work were obtained by using the 'one set of binding sites' models. Two titration experiments were independently performed to give the averaged values with reasonable errors.

Cell culture. Human cervical cancer HeLa cell line, rat kin fibroblast like cells RS1 cell line, and mouse fibroblasts cells L929 cell line were obtained from Institute of Basic Medical Science, Chinese Academy of Medical Science. HeLa, RS1, and L929 were cells were cultured in a cell incubator with a DMEM high-glucose nutrient medium containing 10% fetal bovine serum and 1 % penicillin streptomycin in a humidified standard under 5% CO_2 at 37 °C.

Intracellular ROS imaging: The treated cells were subcultured into a confocal petri dish and incubated for 12 h. In the H_2O_2 treated group, cells were cultured with H_2O_2 (100 μM) in the culture medium for another 24 h. After this, the culture medium was discarded, and the cells were washed with 0.01 M PBS at least three times. Then the cells were incubated with the commercially available probe 6-carboxy-2',7'-dichlorodihydrofluorescein diacetate (DCFH-DA) at 37 °C for 30 min. The cells were repeatedly washed at least three times with PBS. Then the cells were observed by CLSM.

Cell colocalization imaging: The cells were first subcultured into a confocal petri dish and incubated for 24 h. Then cells were treated with PDI, PDI⊂CB[8], PDI/MLGG-6C⊂CB[8] solution that final concentration is 30 μM ([PDI]) in the culture medium and cultured for another 24 h. After this, the culture medium was discarded, and the cells were washed with 0.01 M PBS at least three times. Next, ER Tracker Green cocultured with the cells at 37 °C for 40 min to stain the endoplasmic reticulum. After the cells were repeatedly washed at least three times with PBS, the localization of the nanoparticles in the cells was immediately observed by CLSM.

CCK8 assay: The cells were seeded in 96-well plates at a density of 5×10^4 cells per well in 100 μL culture medium and cultured in 5% CO_2 at 37 °C for 12 h. In the H_2O_2 treated group, cells were cultured with H_2O_2 (100 μM) in the culture medium for another 24 h. After this, the culture medium was discarded, and the cells were washed with 0.01 M PBS at least three times. Then the cells were incubated with PDI, PDI⊂CB[8] complex, MLGG-6C⊂CB[8] complex, PDI/MLGG-6C⊂CB[8] assembly, and further incubated for 24 h, respectively. Then, cells were washed and replenished with fresh culture medium. The cell viability was evaluated by CCK8 assay according to the kit instruction. The plate was then read by a microplate reader at a wavelength of 450 nm. The assembly's concentration was calculated based on the PDI concentration.

2. Synthesis and characterization of target molecules

MLGG-6C: MLGG-6C was synthesized by the Nanjing Genscript Co., Ltd. ^{1}H NMR (400 MHz, D_2O, 25 °C) δ (ppm): 4.43-4.40 (t, J = 4.42 Hz, 1H), 4.15-4.12 (t, J = 4.14 Hz, 1H), 4.01-3.88 (m, J = 3.94 Hz, 4H), 3.25-3.13 (m, J = 3.19 Hz, 2H), 2.65-2.53 (m, J = 2.59 Hz, 2H), 2.19-2.14 (dd, J = 2.16 Hz, 2H), 2.11 (s, 3H), 1.69-1.62 (m, J = 1.65 Hz 3H), 1.50-1.47 (m, J = 1.48 Hz 2H), 1.27 (s, 6H), 0.95-0.90 (m, J = 0.92 Hz, 6H),0.87-0.83 (t, J = 0.85 Hz, 3H). HRMS (ESI): m/z calcd. for $C_{21}H_{41}N_5O_4S$: 459.2879; $[M+H]^+$ found: 460.2955 (calcd. 460.2958).

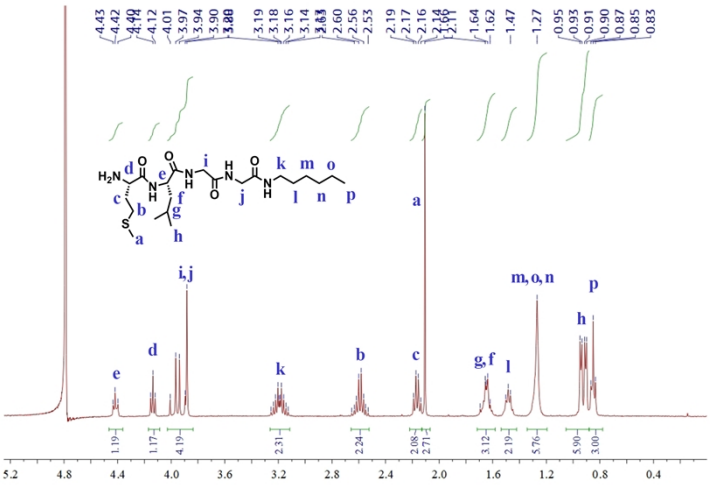

Fig. S1 ^{1}H NMR (400 MHz, D_2O, 298K) spectrum of MLGG-6C.

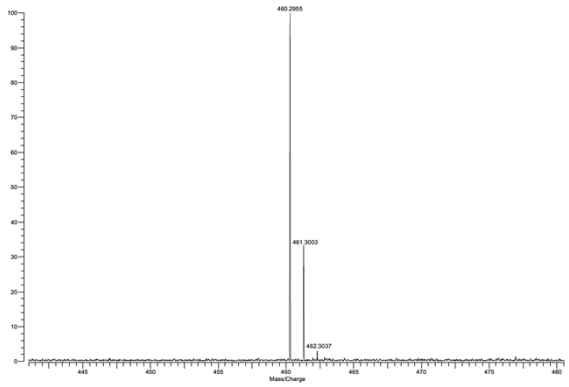

Fig. S2 HRMS of MLGG-6C. The peak at m/z 460.2955 corresponds to $[M + H]^+$ (calcd. 460.2958).

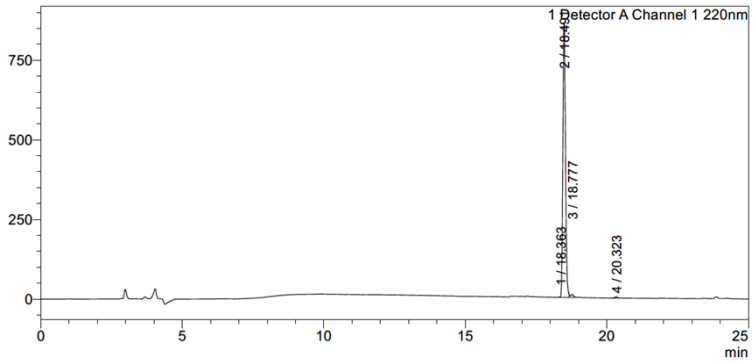

Fig. S3 HPLC of MLGG-6C

Synthesis of peptides: MLGGG, M^{O}LGGG, M^{O2}LGGG, LMGGG, LM^{O}GGG, LM^{O2}GGG was synthesized by the Nanjing Genscript Co., Ltd.

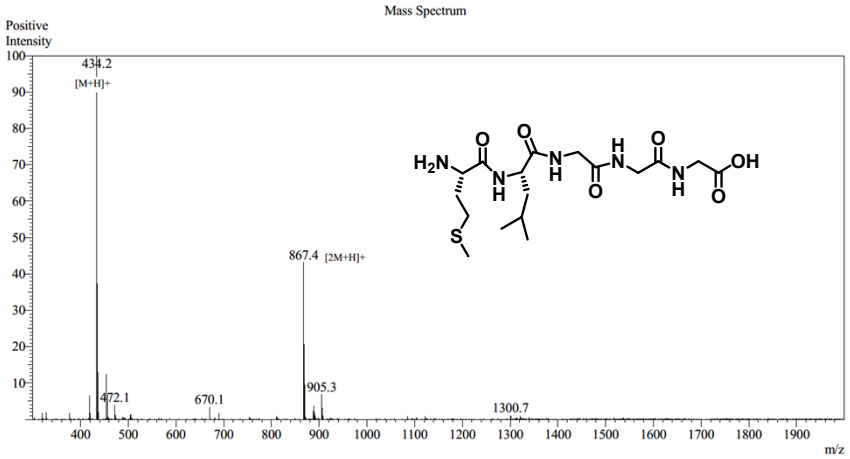

Fig. S4 ESI-MS of MLGGG ($C_{17}H_{31}N_5O_6S$): calcd. *m/z*: 433.20, found: 434.2 ([M + H]$^+$).

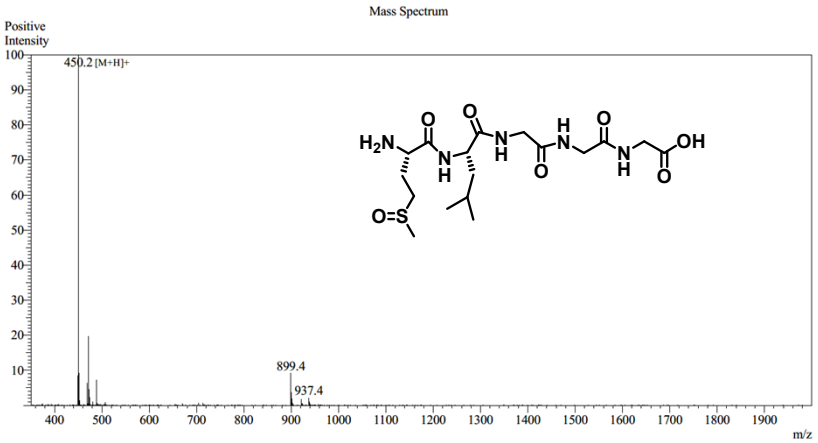

Fig. S5 ESI-MS of M^{O}LGGG ($C_{17}H_{31}N_5O_7S$): calcd. *m/z*: 449.19, found: 450.2 ([M + H]$^+$).

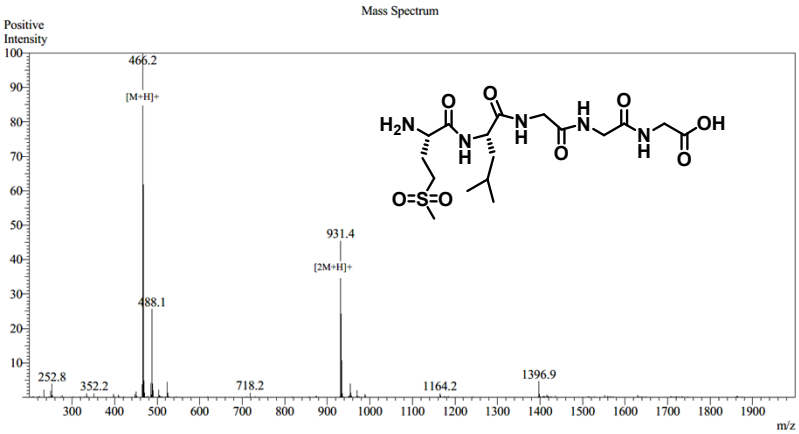

Fig. S6 ESI-MS of M^{O2}LGGG ($C_{17}H_{31}N_5O_8S$): calcd. *m/z*: 456.19, found: 466.2 ([M + H]$^+$).

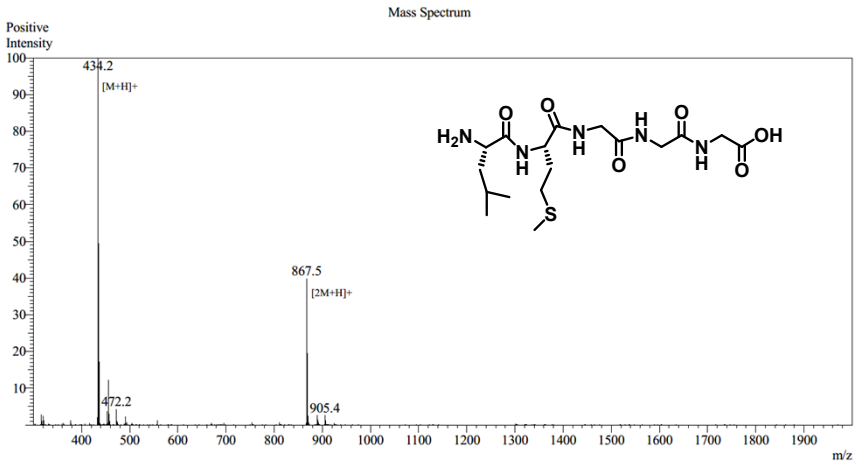

Fig. S7 ESI-MS of LMGGG ($C_{17}H_{31}N_5O_6S$): calcd. *m/z*: 433.20, found: 434.2 ($[M + H]^+$).

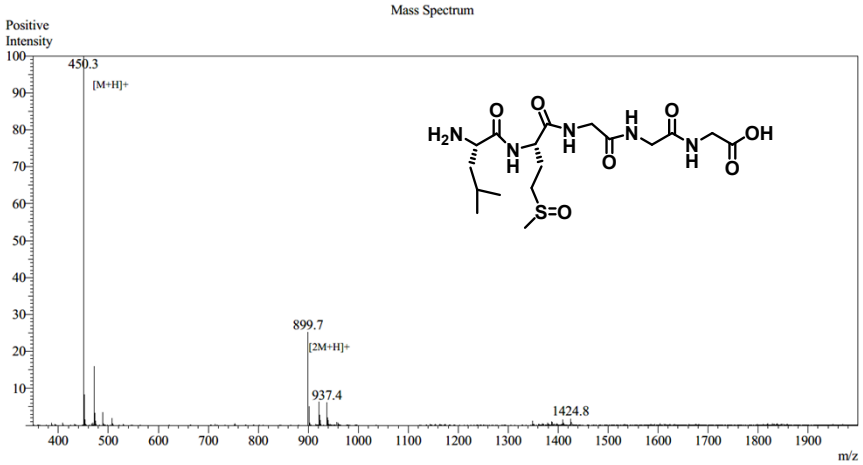

Fig. S8 ESI-MS of LM^{O}GGG ($C_{17}H_{31}N_5O_7S$): calcd. *m/z*: 449.19, found: 450.3 ($[M + H]^+$).

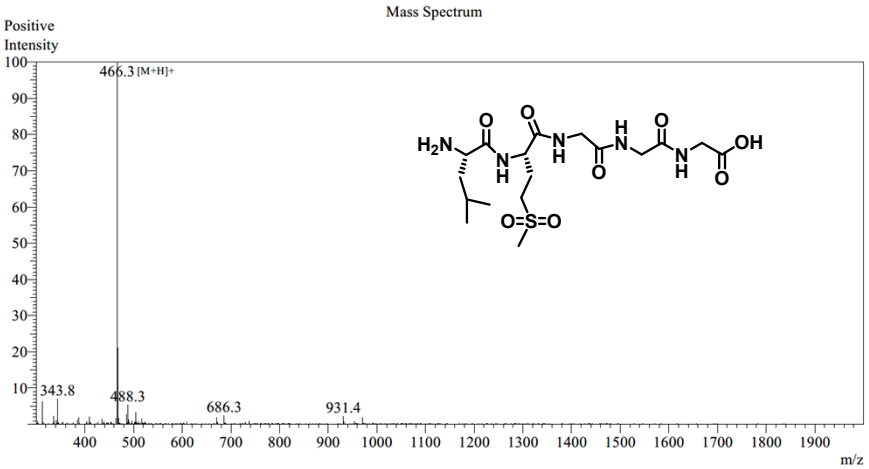

Fig. S9 ESI-MS of LM^{O2}GGG ($C_{17}H_{31}N_5O_8S$): calcd. *m/z*: 456.19, found: 466.3 ($[M + H]^+$).

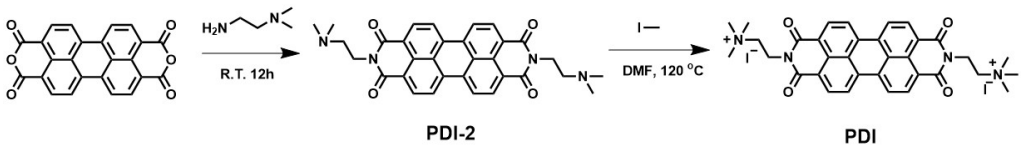

Scheme S1 Synthesis route of PDI

Synthesis of PDI-2: PDI-2 was synthesized according to literature[S2] with a little alteration. The suspension of 3,4,9,10-perylenetetracarboxylic dianhydride (5 g, 12.7 mmol) and 2-dimethylaminoethylamine (10.0 mL, 150 mmol) in anhydrous DMF (50mL) were stirred at 120 ºC under Ar atmosphere for 12 h. After cooling to room temperature, added 200 mL THF were and filtered, collected the precipitate, then washed with THF (100 mL) for three times. Then the solid was vacuumed overnight at 40 °C, the compound was obtained as a dark purple solid with yielded (5.1 g, 10.8 mmol, 95%).

Synthesis of PDI: PDI-2 (1.06 g, 2.0mmol) and methyl iodide (2.82 g, 20.0mmol) were added in anhydrous DMF (20 mL), and the reaction mixture was stirred and reacted at 120 °C under Ar atmosphere for 12 h[S3]. After cooling to room temperature, the reaction mixture was dropped into 200 mL THF, and washed with THF (100 mL) for three times. The solid was dissolved in water (500 mL) and filtered to remove precipitate. The aqueous solution was freeze-drying and yielded the compound as a dark red solid (1.2 g, 1.5 mmol, 75%). ^{1}H NMR (400 MHz, DMSO-d_6, 25 °C) δ (ppm): 8.85-8.83 (d, J = 8.84 Hz, 4H), 8.53-8.51 (d, J = 8.52 Hz, 4H), 4.52-4.48 (t, J = 4.50 Hz, 4H), 3.70-3.66 (t, J = 3.68 Hz, 4H), 3.26 (s, 48H). HRMS (ESI): $C_{34}H_{34}N_4O_4^{2+}$, 562.2569; found: 281.1285 (calcd. m/z: 281.1285).

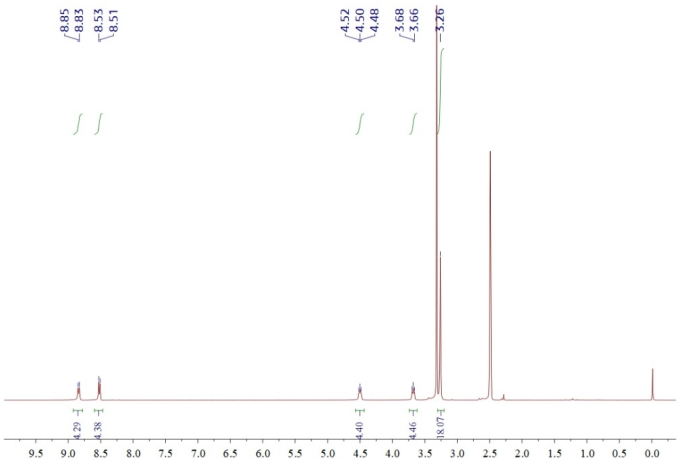

Fig. S10 ^{1}H NMR (400 MHz, DMSO-d_6, 298K) spectrum of PDI.

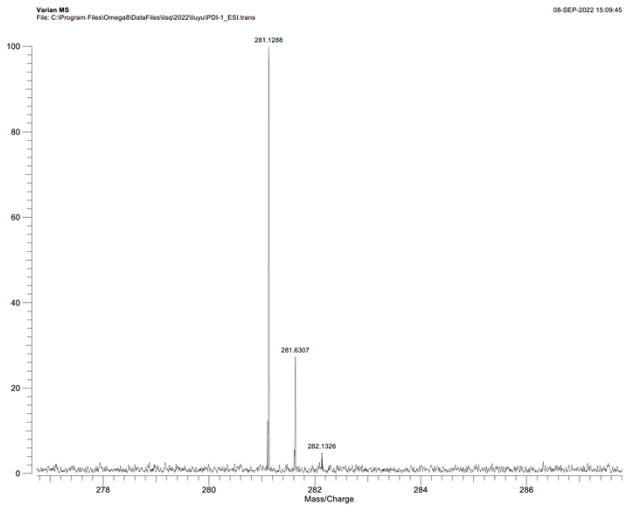

Fig. S11 HRMS of PDI ($C_{34}H_{34}N_4O_4^{2+}$): calcd. *m*/*z*: 281.1285, found: 281.1288.

3. ^{1}H NMR of peptides and CB[8]

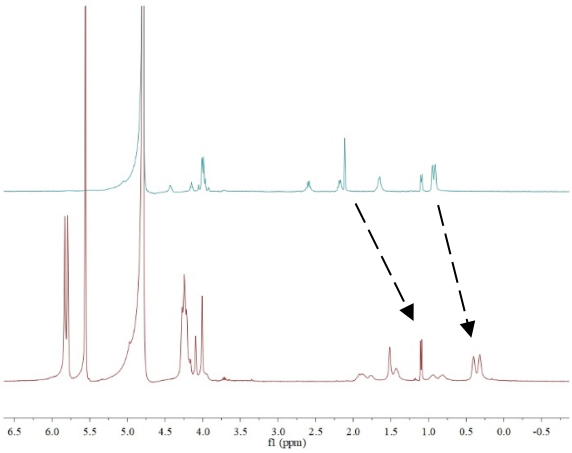

Fig. S12 ^{1}H NMR (400 MHz, D_2O, 298 K) of MLGGG (top) and MLGGG with CB[8] (bottom) ([MLGGG] = 1 mM, [CB[8]] = 1 mM).

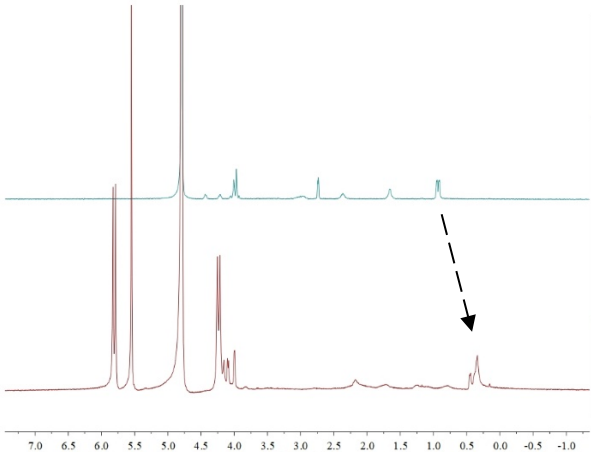

Fig. S13 ^{1}H NMR (400 MHz, D_2O, 298 K) of M^{O}LGGG (top) and M^{O}LGGG with CB[8] (bottom) ([MLGGG] = 1 mM, and [CB[8]] = 1 mM).

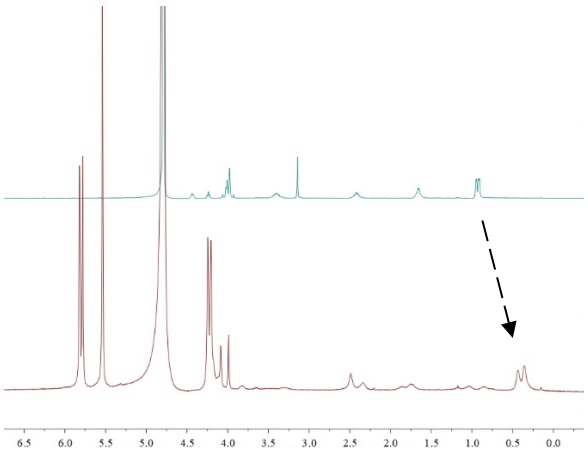

Fig. S14 ^{1}H NMR (400 MHz, D_2O, 298 K) of M^{O2}LGGG (top) and M^{O2}LGGG with CB[8] (bottom) ([MLGGG] = 1 mM, [CB[8]] = 1 mM).

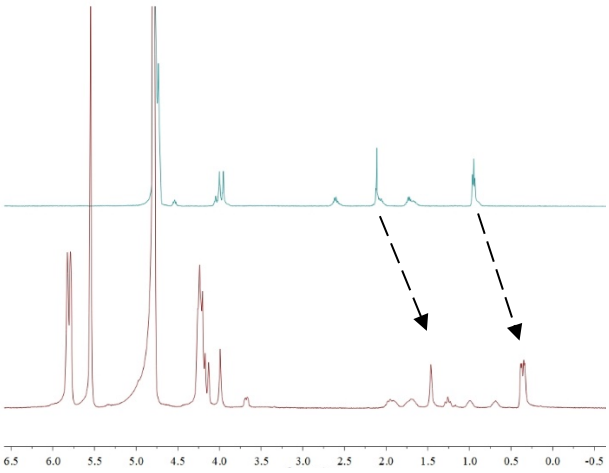

Fig. S15 ^{1}H NMR (400 MHz, D_2O, 298 K) of LMGGG (top) and LMGGG with CB[8] (bottom) ([LMGGG] = 1mM, [CB[8]] = 1 mM).

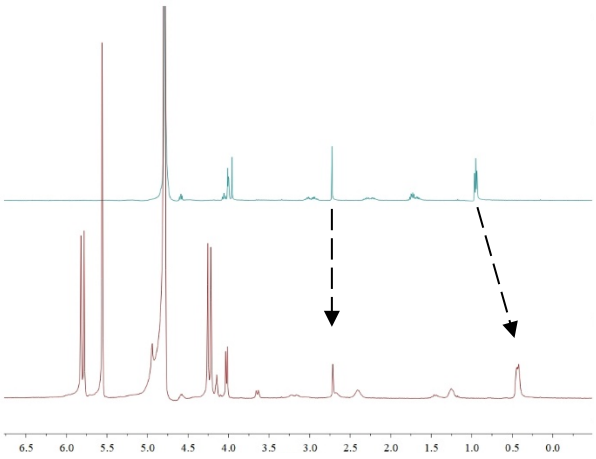

Fig. S16 ^{1}H NMR (400 MHz, D_2O, 298 K) of $LM^{O}GGG$ (top) and $LM^{O}GGG$ with CB[8] (bottom) ([$LM^{O}GGG$] = 1 mM, and [CB[8]] = 1 mM).

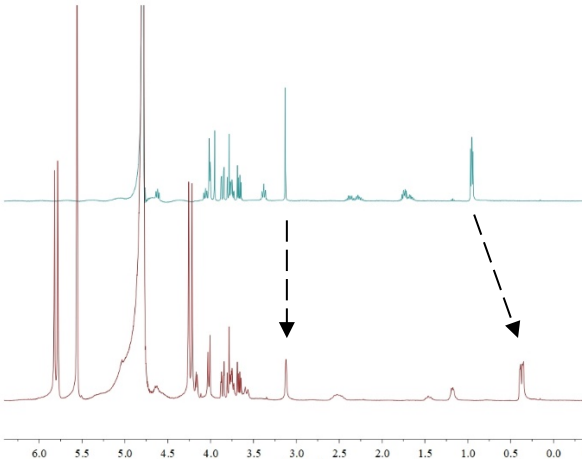

Fig. S17 ^{1}H NMR (400 MHz, D_2O, 298 K) of $LM^{O2}GGG$ (top) and $LM^{O2}GGG$ with CB[8] (bottom) ([$LM^{O2}GGG$] = 1mM, [CB[8]] = 1 mM).

4. ITC spectra of peptides and CB[8]

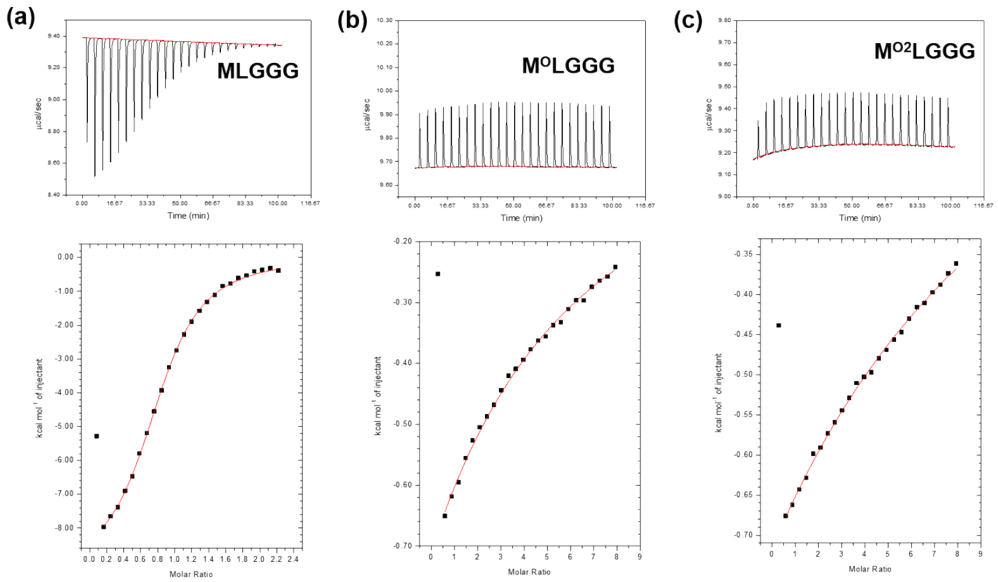

Fig. S18 ITC isotherms for the titration of peptides with CB[8] at 298 K in PBS (pH 7.3, 10 mM), (a) MLGGG with CB[8], (b) M^{O}LGGG, (c) M^{O2}LGGG with CB[8] ([MLGGG] = 0.7 M, [M^{O}LGGG] = 1.25 mM [M^{O2}LGGG] = 1.25 mM, and [CB [8]] = 0.04 mM).

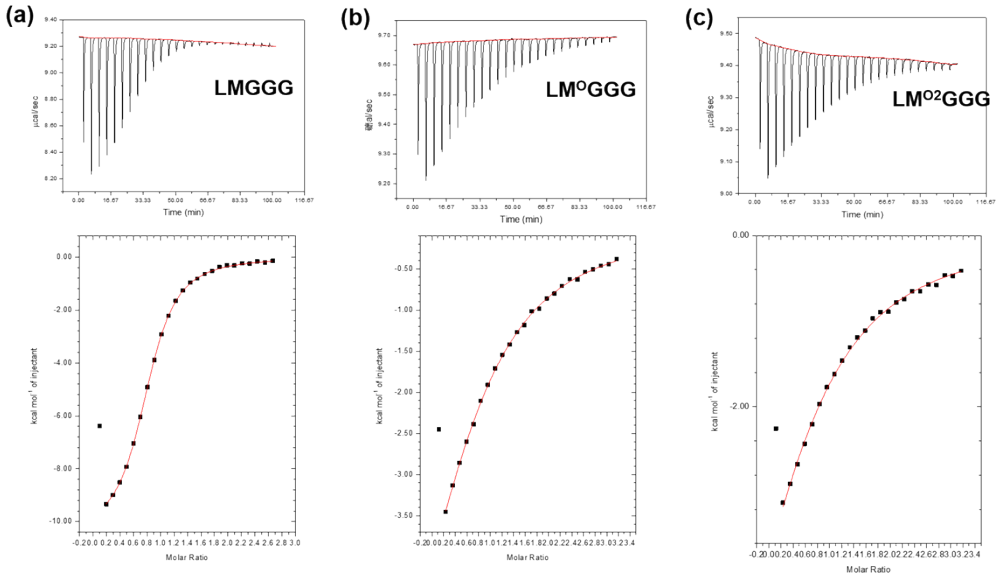

Fig. S19 ITC isotherms for the titration of peptides with CB[8] at 298 K in PBS (pH 7.3, 10 mM), (a) LMGGG with CB[8], (b) LM^{O}GGG, (c) LM^{O2}GGG with CB[8] ([LMGGG] = 0.7 M, [LM^{O}GGG] = 1.0 mM [M^{O2}LGGG] = 1.0 mM, and [CB [8]] = 0.04 mM).

5. Electrostatic potential surfaces of peptides

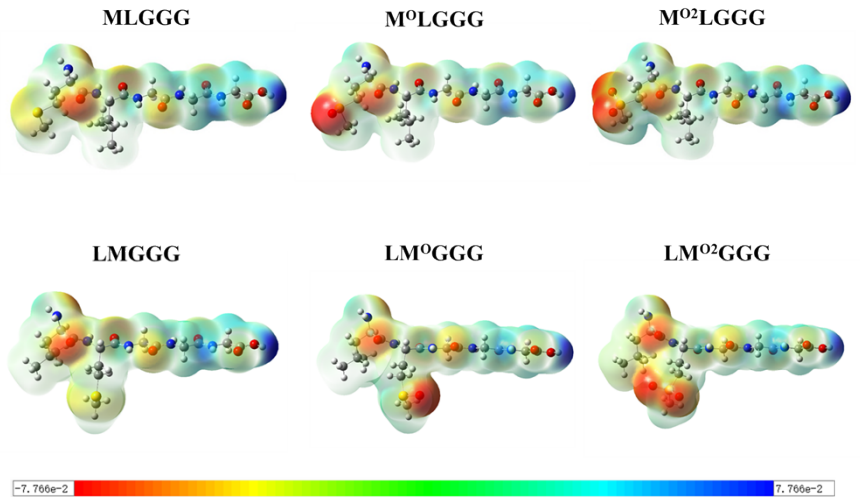

Fig. S20 Electrostatic potential surfaces of peptides. Blue and red represent positive and negative electrostatic potentials, respectively. DFT calculations were performed at B3LYP/6-31G// using Gaussian09.

6. Characterization of M^{O}LGG-6C

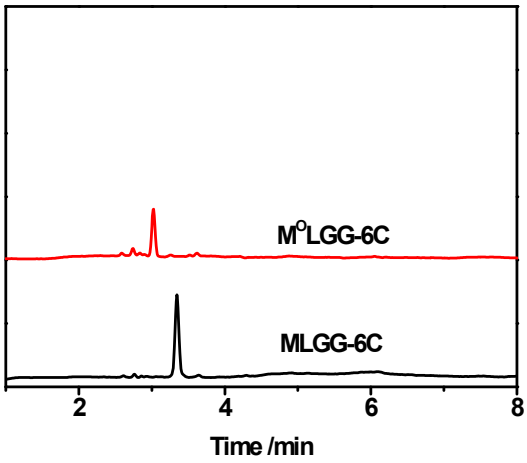

Fig. S21 HPLC traces of (bottom) MLGG-6C and (top) MLGG-6C with H_2O_2

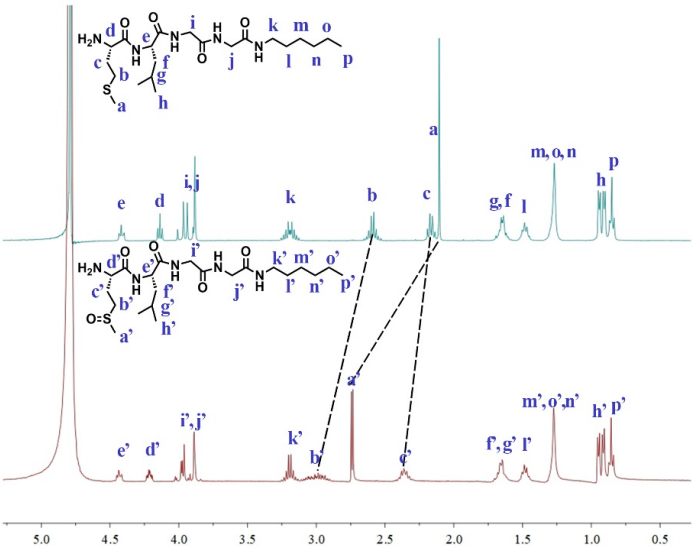

Fig. S22 ^{1}H NMR (400 MHz, D_2O, 298 K) of MLGG-6C (top) and MLGG-6C with 3 eq H_2O_2 (bottom). [MLGG-6C] = 1 mM

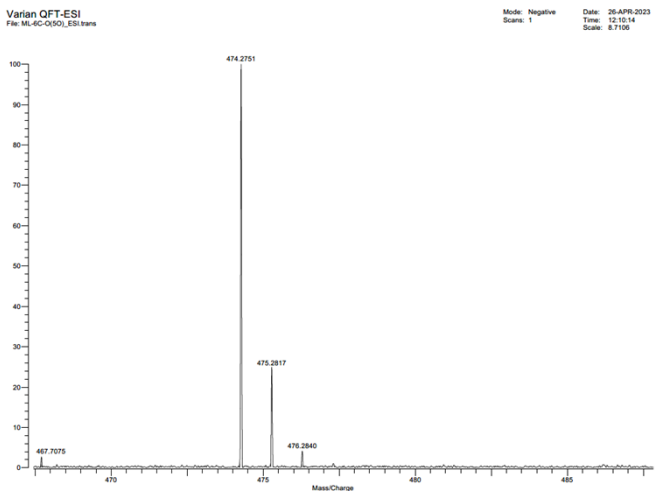

Fig. S23 HRMS of M^{O}LGG-6C. The peak at *m*/*z* 474.2751 corresponds to $[M-H]^-$ (calcd. 474.2755)

7. Electrostatic potential surfaces of MLGG-6C and M^{O}LGG-6C

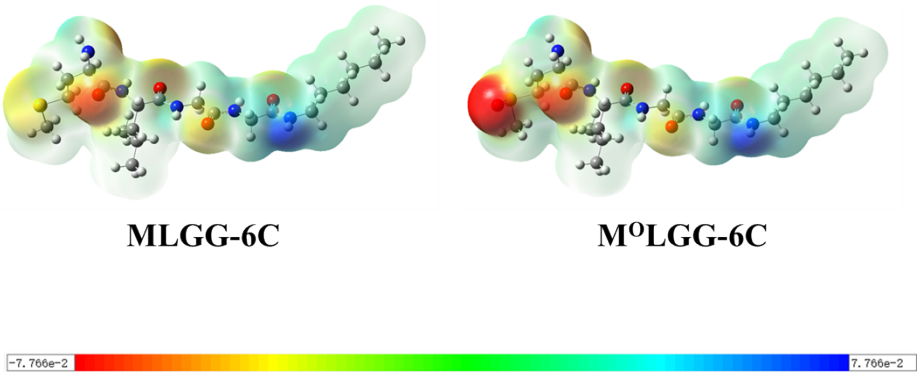

Fig. S24 Electrostatic potential surfaces of MLGG-6C and M^{O}LGG-6C. Blue and red represent positive and negative electrostatic potentials, respectively. DFT calculations were performed at B3LYP/6-31G// using Gaussian09.

8. UV-Vis titration, ITC titration and fluorescence spectra of CB[8] and PDI

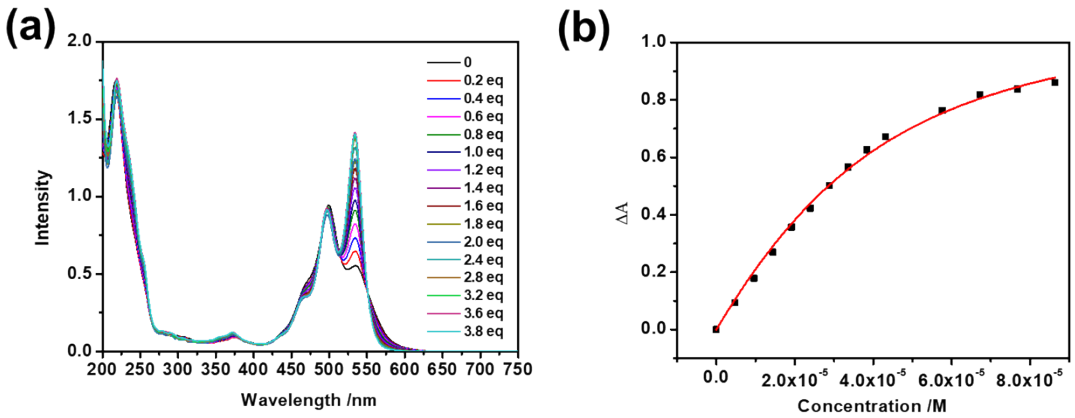

Fig. S25 (a) UV-Vis absorbance spectra of PDI with CB[8] ([PDI] = 30 μM). The molar ratios of CB[8]/PDI were 0, 0.2, 0.4, 0.6, 0.8 1.0, 1.2, 1.4, 1.6, 1.8, 2.0, 2.4, 2.8, 3.2, 3.6, 3.8, respectively, (b) The nonlinear curve fitting of the variation of UV-Vis absorbance at 534 nm of PDI with the concentrations of CB[8] to calculate the binding constants.

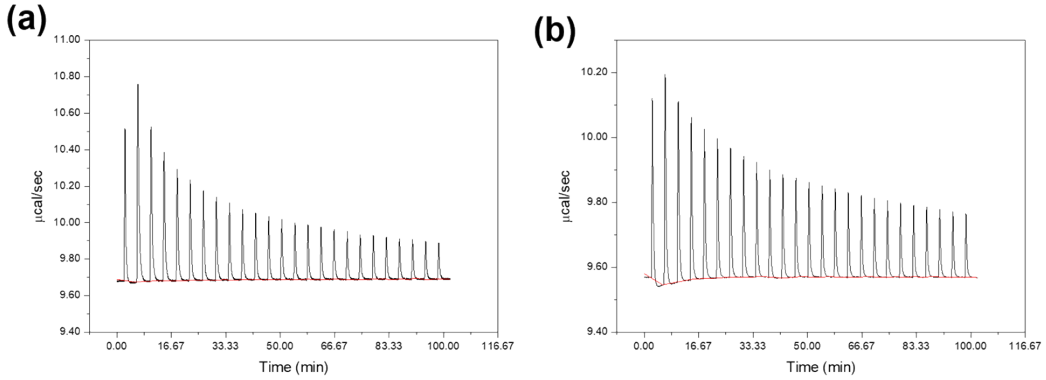

Fig. S26 Raw ITC thermograms for (a) heat of complexation and (b) heat of dilution for the titration of PDI with CB[8] at 298 K ([PDI] = 0.8 mM and [CB[8]] = 0.03 mM).

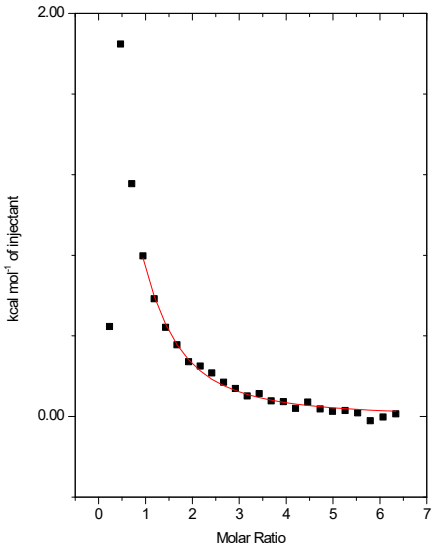

Fig. S27 ITC curves obtained for the titration of PDI with CB[8] at 298 K ([PDI] = 0.8 mM and [CB[8]] = 0.03 mM).

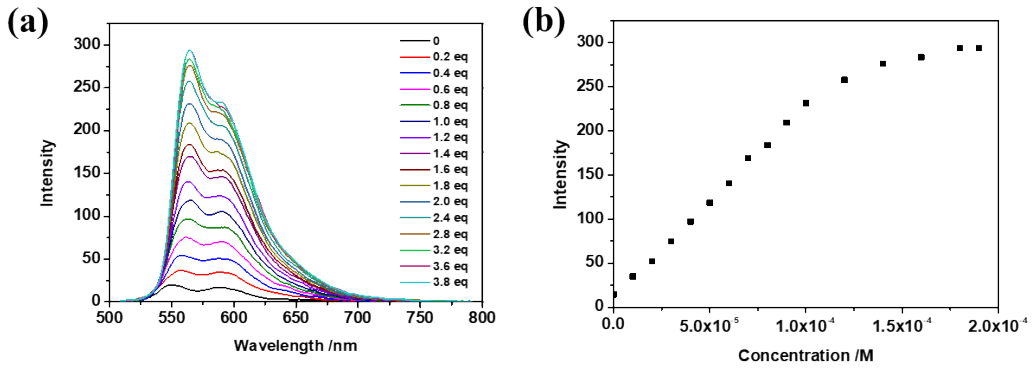

Fig. S28 (a) Fluorescence emission spectra of PDI with CB[8] ([PDI] = 50 μM). The molar ratios of CB[8]/PDI were 0, 0.2, 0.4, 0.6, 0.8 1.0, 1.2, 1.4, 1.6, 1.8, 2.0, 2.4, 2.8, 3.2, 3.6, 3.8, respectively. (b)The intensity of PDI at 563 nm with the concentrations of CB[8].

9. 2D DOSY NMR spectra of CB[8] and PDI

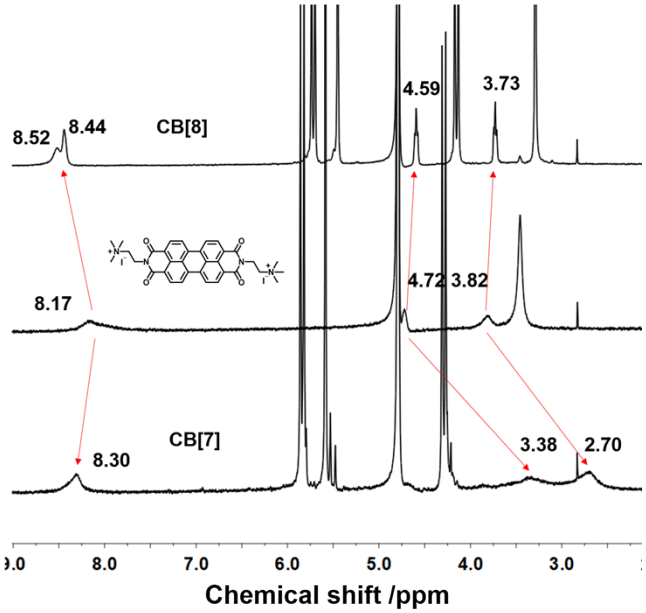

Fig. S29 ^{1}H NMR spectra of PDI, PDI⊂CB[8] complex, PDI⊂CB[7] complex in D_2O ([PDI] = 1.0 mM, [CB[8]] = 1.0 mM, and [CB[7]] = 2.0 mM).

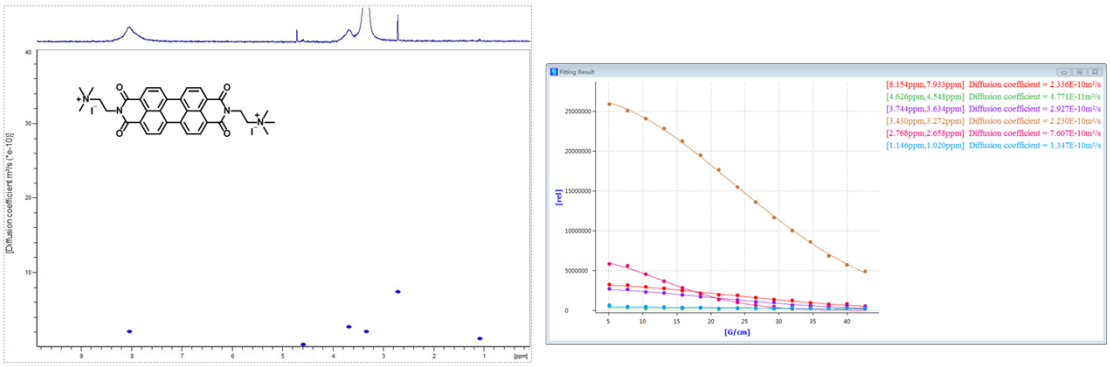

Fig. S30 2D DOSY NMR spectrum (400 MHz, D_2O, 298 K) of PDI ([PDI] = 1.0 mM).

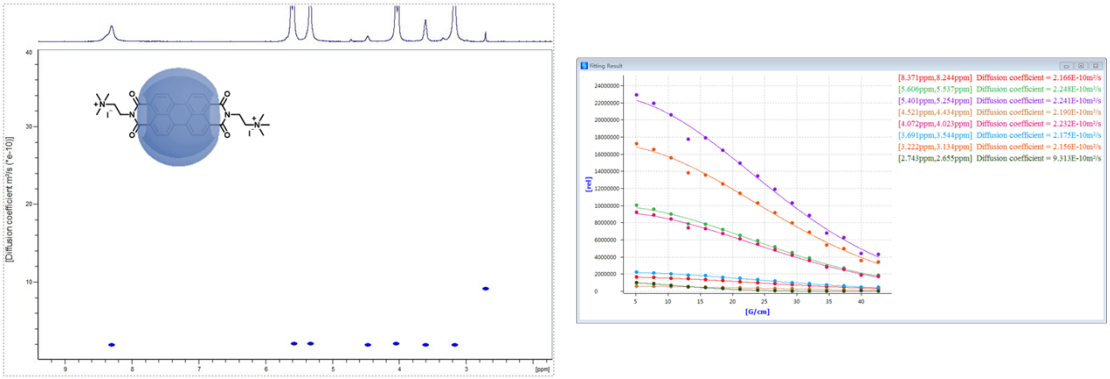

Fig. S31 2D DOSY NMR spectrum (400 MHz, D_2O, 298 K) of PDI⊂CB[8] complex ([PDI] = 1.0 mM and [CB[8]] = 1.0 mM).

10. Fluorescence spectra spectra of CB[7] and PD

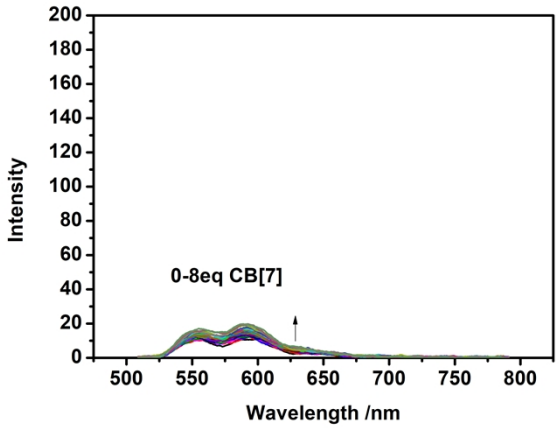

Fig. S32 Fluorescence emission spectra of PDI in water with addition of CB[8] at 298 K ([PDI] = 50 μM, [CB[7]] = 0-400 μM).

11. Fluorescence spectra for adding MLGG-6C to PDI⊂CB[8] and PDI

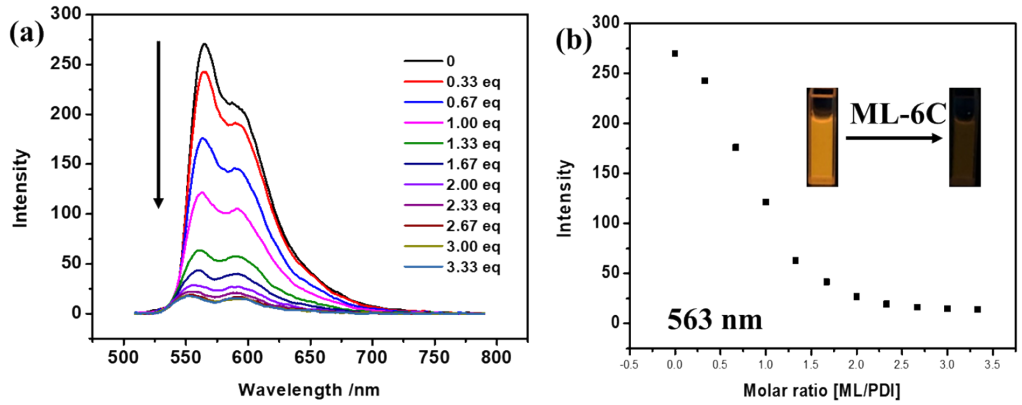

Fig. S33 (a) Fluorescence emission spectra of adding MLGG-6C to PDI⊂CB[8] ([PDI] = 50 μM, [CB[8]] = 150 μM). The molar ratios of MLGG-6C/PDI were 0, 0.33, 0.67, 1.00, 1.33, 1.67, 2.00, 2.33, 2.67, 3.00, 3.33, respectively. (b)The Intensity of PDI at 563 nm with different concentrations of MLGG-6C.

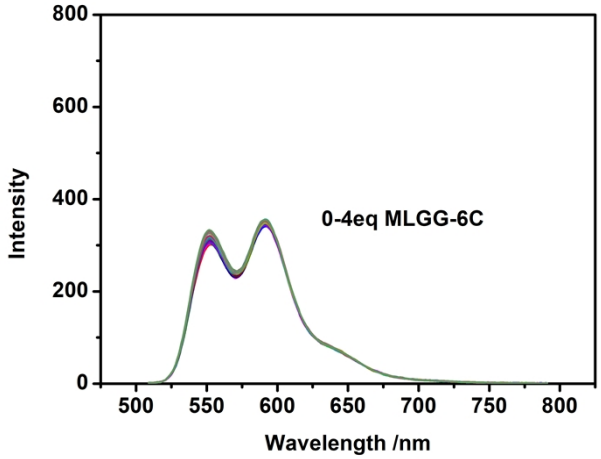

Fig. S34 Fluorescence emission spectra of PDI in water with addition of MLGG-6C at 298 K ([PDI] = 50 μM and [MLGG-6C] = 0-200 μM).

12. UV-Vis absorbance, and ITC titration spectra for adding MLGG-6C to PDI⊂CB[8]

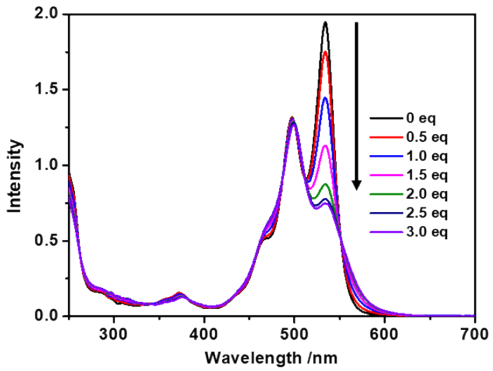

Fig. S35 UV-Vis absorbance spectra of adding MLGG-6C to PDI⊂CB[8] ([PDI] = 30 μM, [CB[8]] = 90 μM). The molar ratios of MLGG-6C/PDI were 0, 0.5, 1.0, 1.5, 2.0, 2.5, 3.0, respectively.

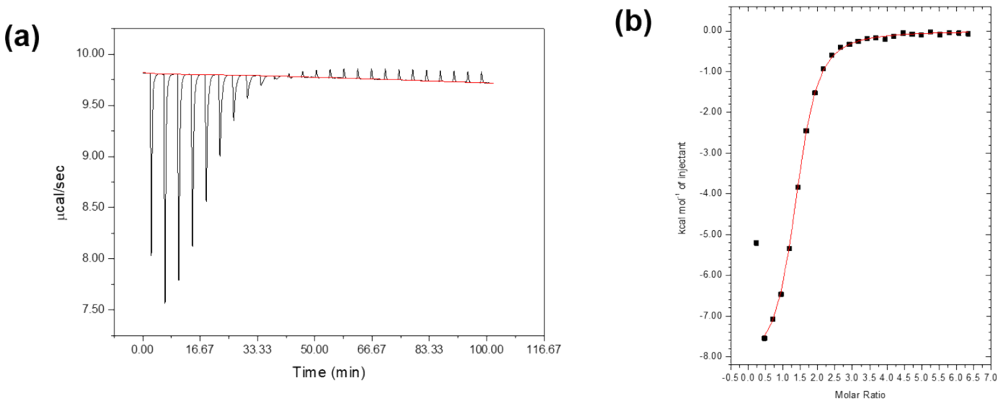

Fig. S36 Raw ITC thermograms for heat of complexation of MLGGG with PDI⊂CB[8] complex at 298 K ([MLGGG] = 1.0 mM, [PDI] = [CB[8]] = 0.03 mM). Through the competitive binding method, the K_S of MLGGG⊂CB[8] complexation was calculated as 9.01×10^5 M^{-1}.[S4]

13. Stability test of PDI

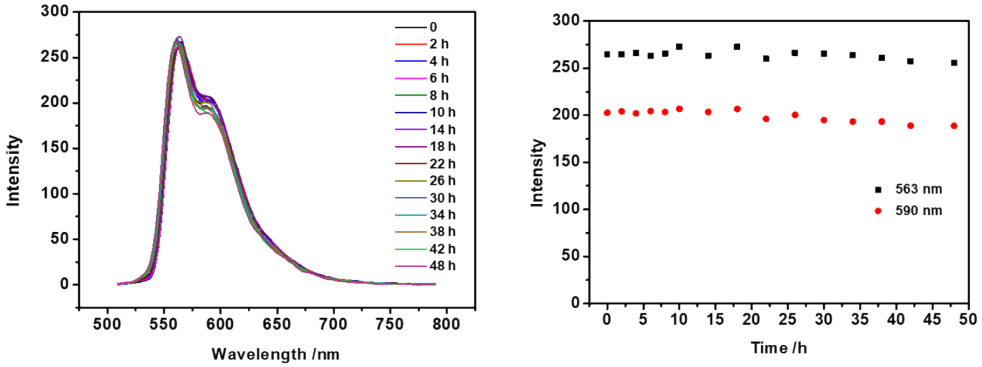

Fig. S37 (left) fluorescence spectrum of PDI⊂CB[8] with 1 mM H_2O_2 at 37 °C, and (right) Time-dependent intensity at 563 nm, 590 nm ([PDI] = 50 μM, [CB [8]] = 150 μM).

14. Quantum yield spectra of PDI

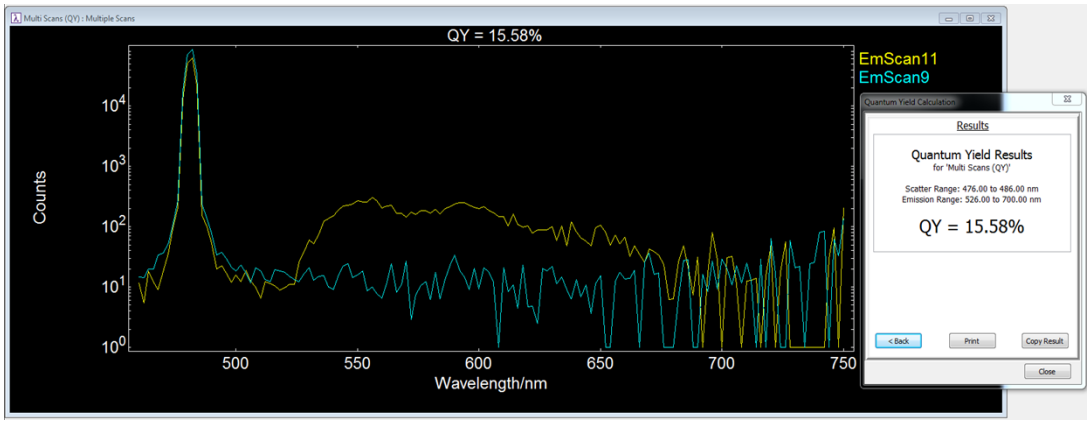

Fig. S38 Quantum yield spectrum of PDI ([PDI] = 10 μM).

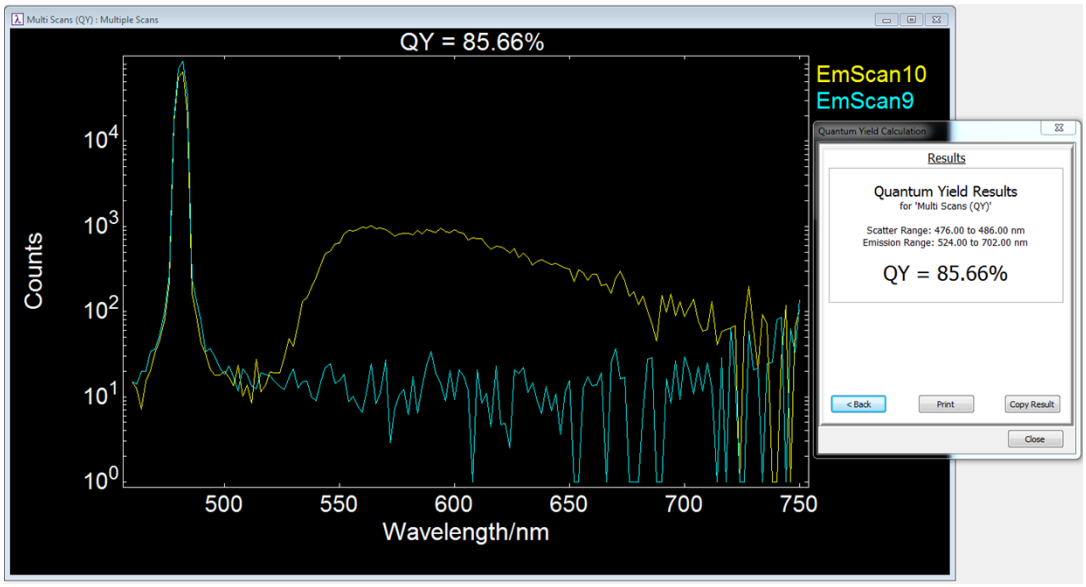

Fig. S39 Quantum yield spectrum of PDI⊂CB[8] ([PDI] = 10 μM, [CB [8]] = 30 μM).

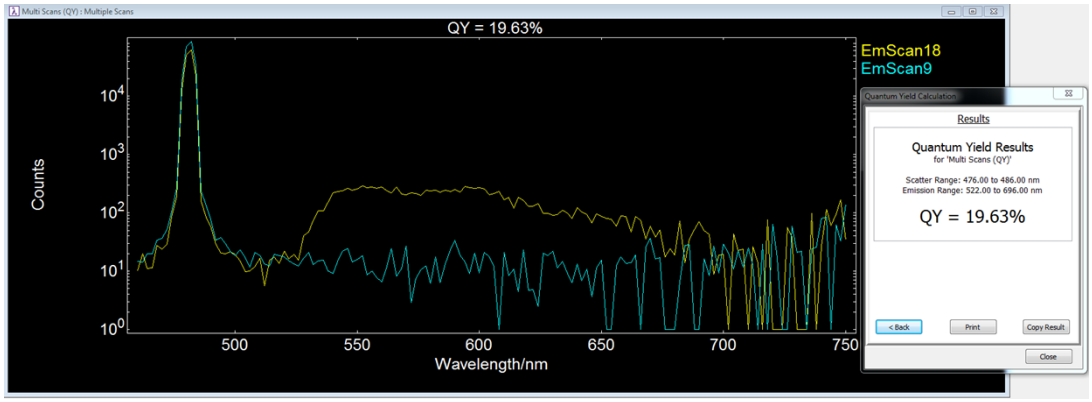

Fig. S40 Quantum yield spectrum of PDI/MLGG-6C⊂CB[8] ([PDI] = 10 μM, [CB [8]] = 30 μM, [MLGG-6C] = 30 μM).

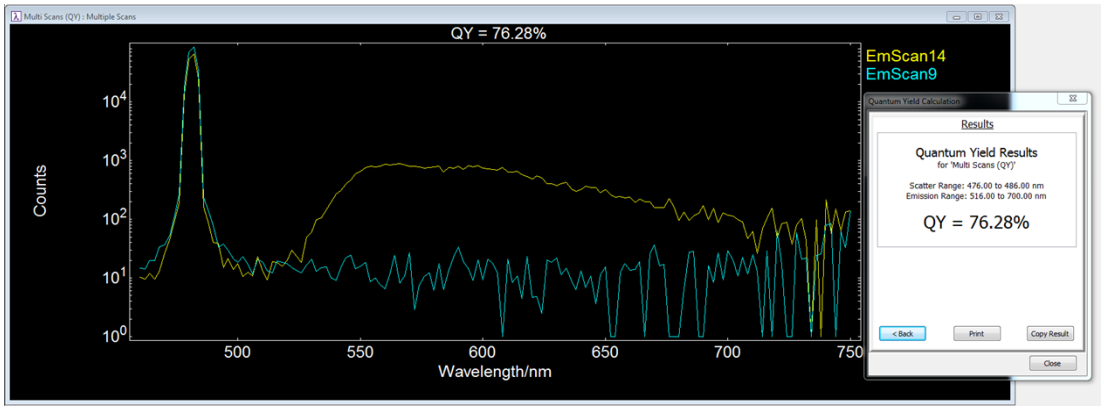

Fig. S41 Quantum yield spectrum of oxidation PDI/MLGG-6C⊂CB[8] ([PDI] = 10 μM, [CB[8]] = 30 μM, [MLGG-6C] = 30 μM, [H_2O_2] = 1 mM).

15. Fluorescence lifetime spectra of PDI

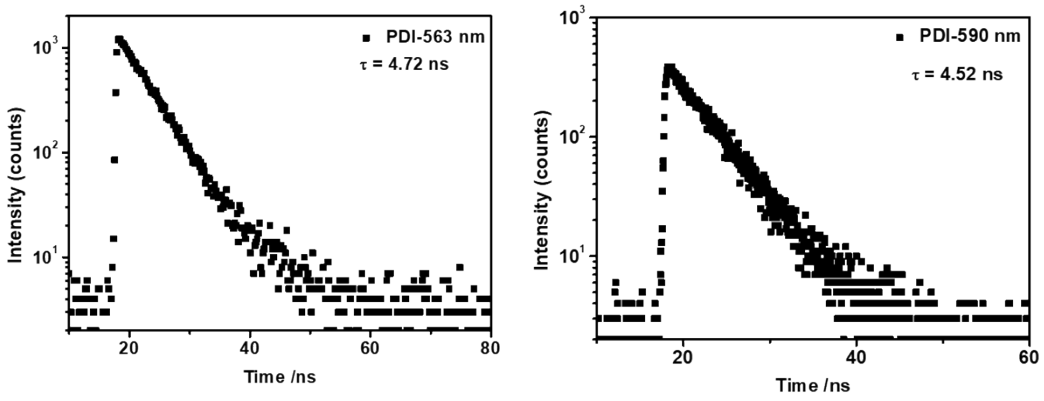

Fig. S42 Fluorescence lifetime decay curves of PDI at 563 nm, 590 nm ([PDI] = 50 μM, [CB [8]] = 150 μM).

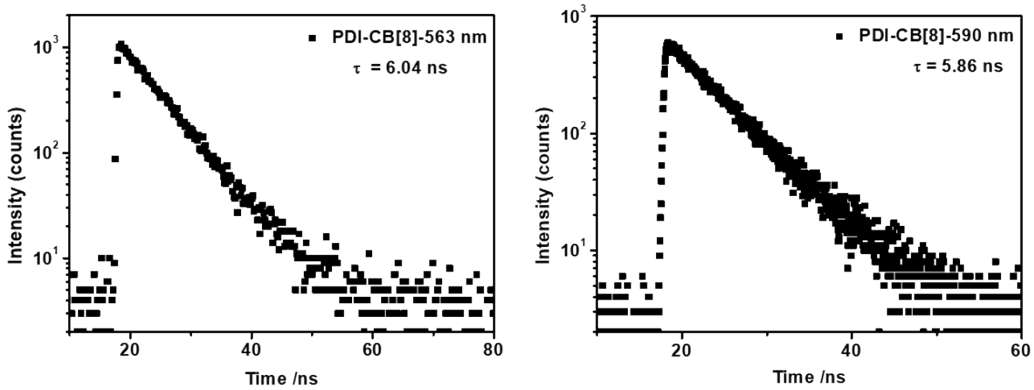

Fig. S43 Fluorescence lifetime decay curves of PDI⊂CB[8] at 563 nm, 590 nm ([PDI] = 50 μM, [CB [8]] = 150 μM).

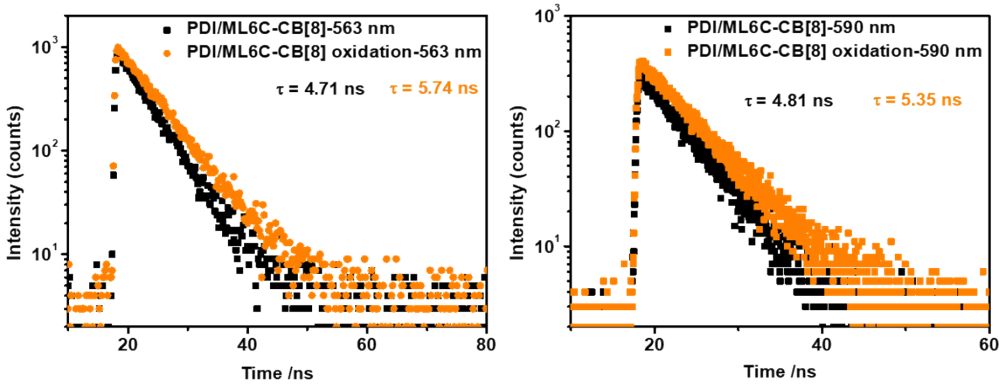

Fig. S44 Fluorescence lifetime Fluorescence lifetime decay curves of PDI/MLGG-6C⊂CB[8] assembly before and after oxidation at (right) 563 and (left) 590 nm; ([PDI] = 50 μM, [CB [8]] = 150 μM, [MLGG-6C] = 150 μM).

Table S1 Quantum yield and fluorescence lifetime of PDI

Sample	**QY**	**τ 563 nm**	**τ 590 nm**
PDI	15.58 %	4.72 ns	4.52 ns
PDI-CB[8]	85.66 %	6.04 ns	5.86 ns
ML6C-PDI-CB[8]	19.63 %	4.71 ns	4.81 ns
ML6C-PDI-CB[8]-oxidation	76.28 %	5.74 ns	5.35 ns

16. Oxidation properties of YLGGG and CLGGG peptides

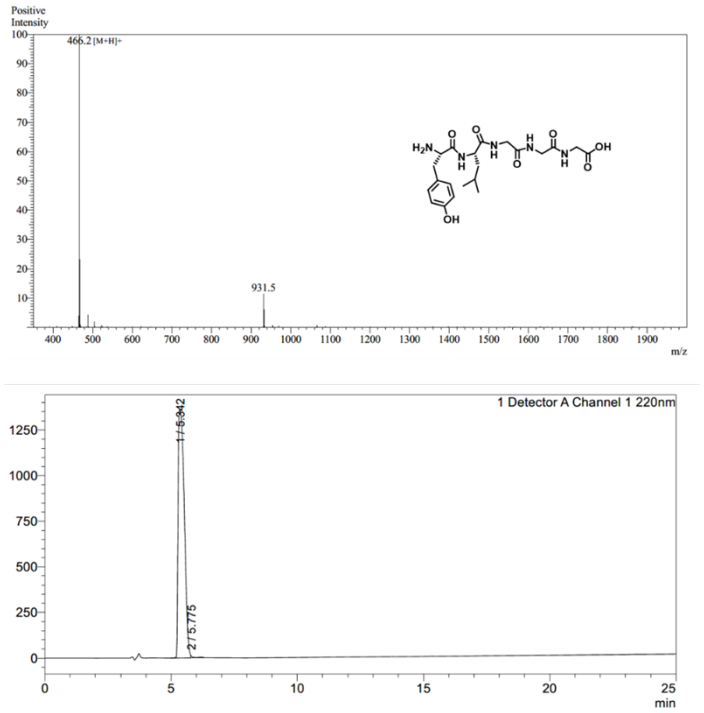

Fig. S45 (top) ESI-MS spectrum of YLGGG, the peak at *m*/*z* 466.2 corresponds to $[M + H]^+$ (calcd. 466.2), (bottom) HPLC of YLGGG.

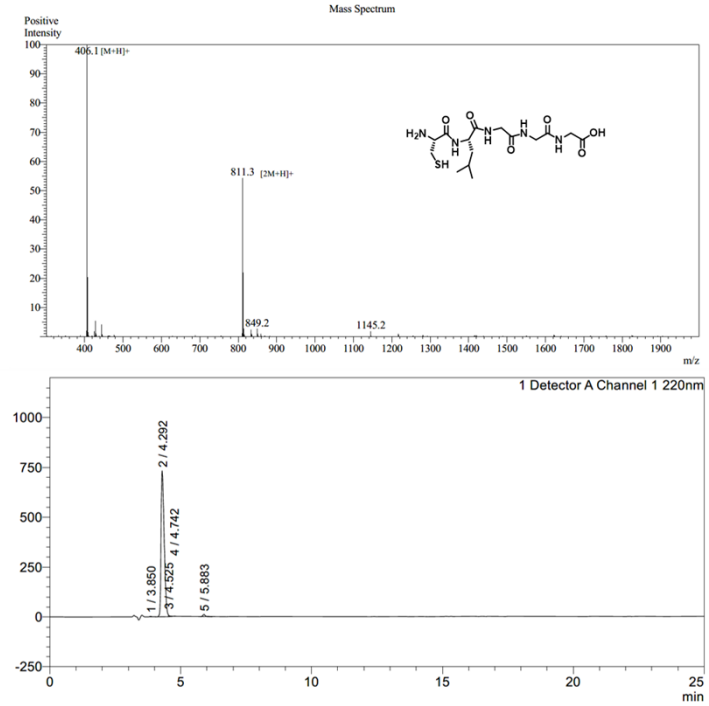

Fig. S46 (top) ESI-MS spectrum of CLGGG, the peak at *m*/*z* 406.1 corresponds to $[M + H]^+$ (calcd. 406.2), (bottom) HPLC of CLGGG.

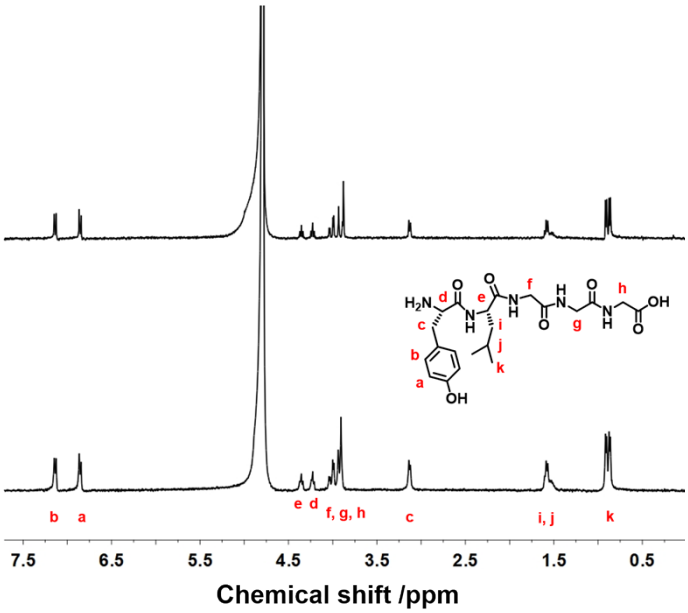

Fig. S47 ^{1}H NMR spectra (400 MHz, D_2O, 298 K) of (bottom) YLGGG and (top) YLGGG with 3 equiv. H_2O_2 ([YLGGG] = 1 mM).

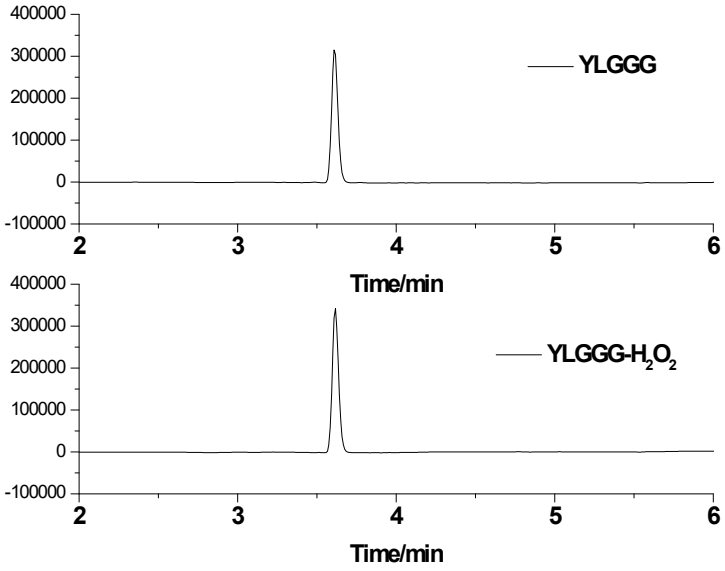

Fig. S48 HPLC traces of YLGGG (top) and YLGGG (bottom) with H_2O_2.

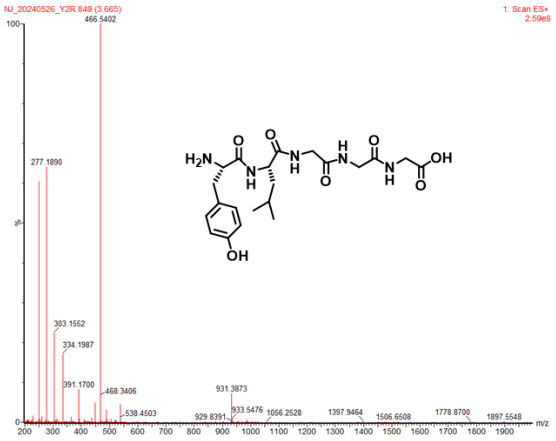

Fig. S49 ESI-MS spectrum of YLGGG. The peak at *m/z* 466.54 corresponds to $[M+H]^+$ (calcd. 466.23).

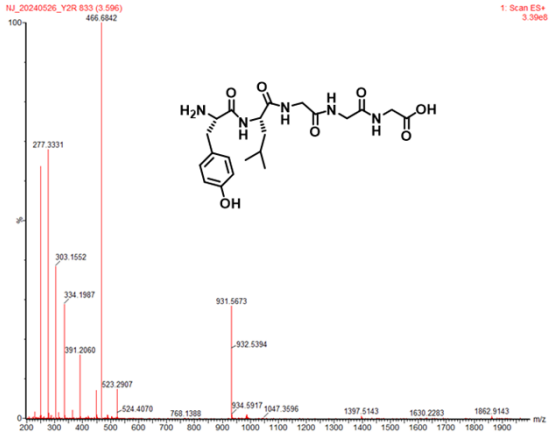

Fig. S50 ESI-MS spectrum of YLGGG with H_2O_2. The peak at *m/z* 466.68 corresponds to $[M + H]^+$ (calcd. 466.23).

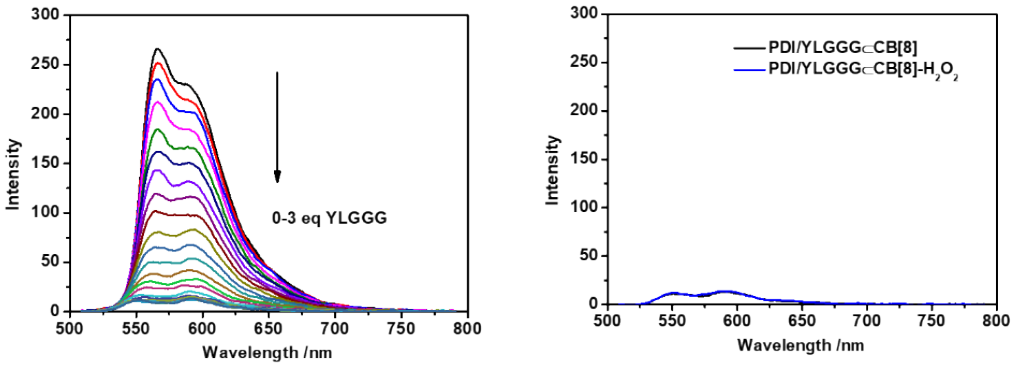

Fig. S51 (a) Fluorescence emission spectra of adding YLGGG to PDI⊂CB[8] complex ([PDI] = 50 μM, [CB[8]] = 150 μM, and [YLGGG] = 0–150μM). (b) Fluorescence emission spectra of PDI/YLGGG⊂CB[8] assembly in water containing H_2O_2.

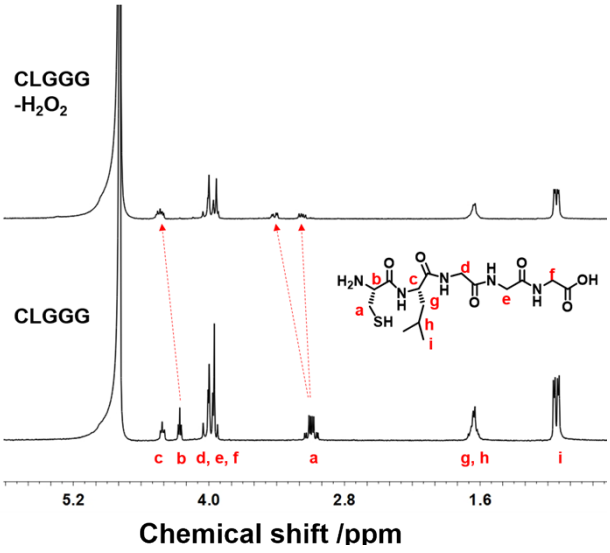

Fig. S52 ^{1}H NMR spectra (400 MHz, D_2O, 298 K) of (bottom) CLGGG and (top) CLGGG with 3 eq H_2O_2 ([CLGGG] = 1 mM).

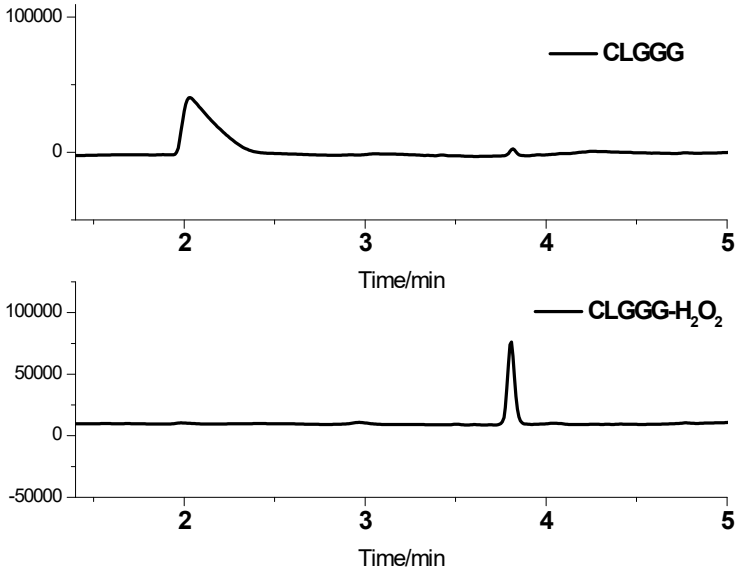

Fig. S53 HPLC traces of CLGGG (top) and CLGGG (bottom) with H_2O_2.

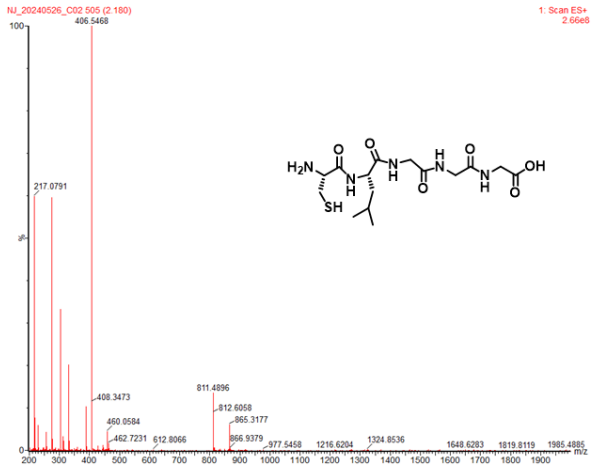

Fig. S54 ESI-MS spectrum of CLGGG. The peak at *m/z* 406.55 corresponds to $[M + H]^+$ (calcd. 406.17).

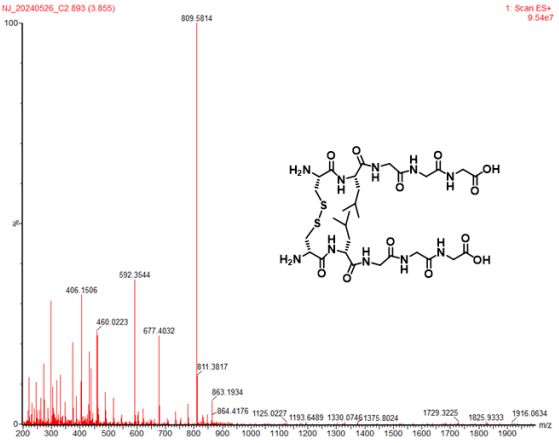

Fig. S55 ESI-MS spectrum of CLGGG with H_2O_2. The peak at *m/z* 809.58 corresponds to $[2M - H]^+$ (calcd. 809.33).

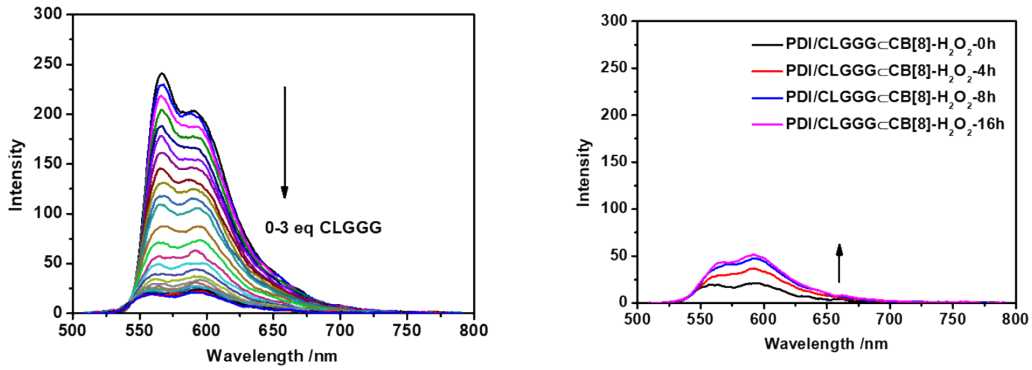

Fig. S56 (a) Fluorescence emission spectra by adding CLGGG to PDI⊂CB[8] complex ([PDI] = 50 μM, [CB[8]] = 150 μM, and [CLGGG] = 0–150 μM). (b) Fluorescence emission spectra of PDI/CLGGG⊂CB[8] assembly in water containing H_2O_2.

17. TEM images of MLGG and PDI with CB[8]

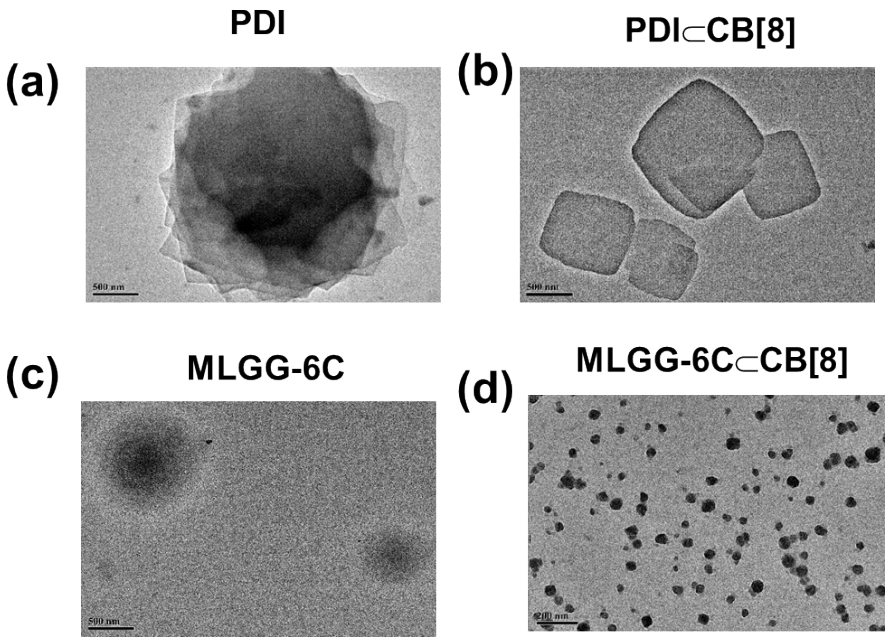

Fig. S57 TEM images of MLGG-6C, MLGG-6C⊂CB[8], PDI, and PDI⊂CB[8].

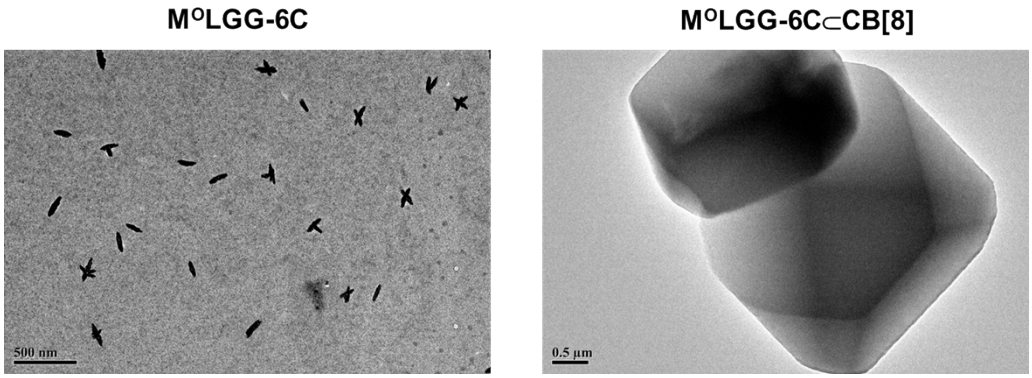

Fig. S58 TEM images of M^{O}LGG-6C and M^{O}LGG-6C⊂CB[8] complex.

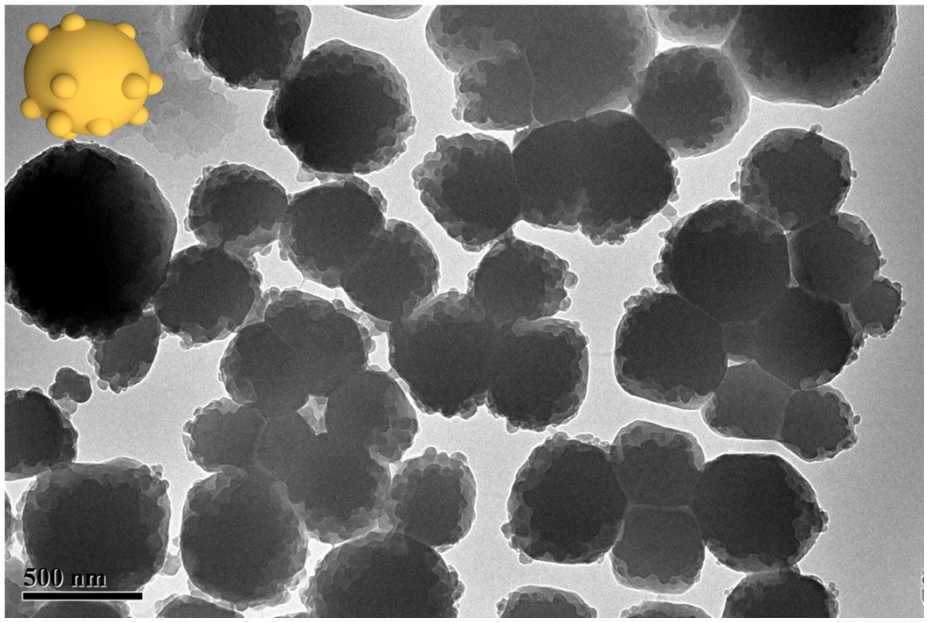

Fig. S59 TEM images of assembly structures in morphology transformation process. Inset: the cartoon representation of satellite-like nanoparticles around large-sized assembly.

18. TEM images of PDI/MLGG-6C⊂CB[8] at different pH

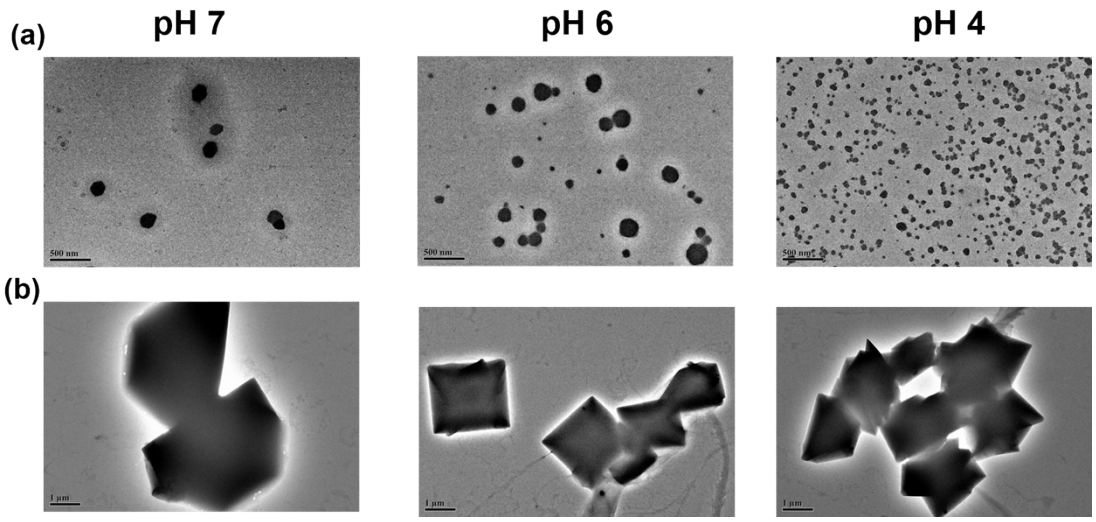

Fig. S60 TEM images of PDI/MLGG-6C⊂CB[8] assembly before (a) and after (b) oxidation by H_2O_2 at pH 7, 6, and 4.

19. Fluorescence and TEM of PDI/MLGG-6C⊂CB[8] assembly

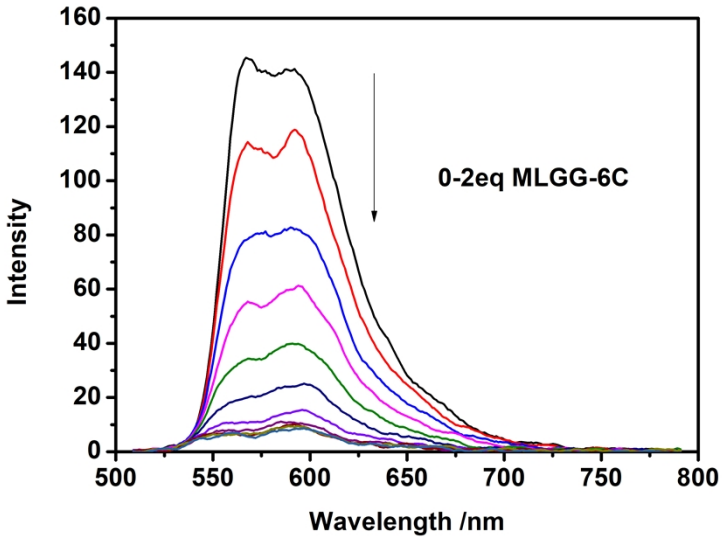

Fig. S61 Fluorescence emission spectra of PDI⊂CB[8] complex in water with addition of 2 equiv. MLGG-6C at 298 K ([PDI] = 50 μM, [CB[8]] = 100 μM, and [MLGG-6C] = 0–100 μM).

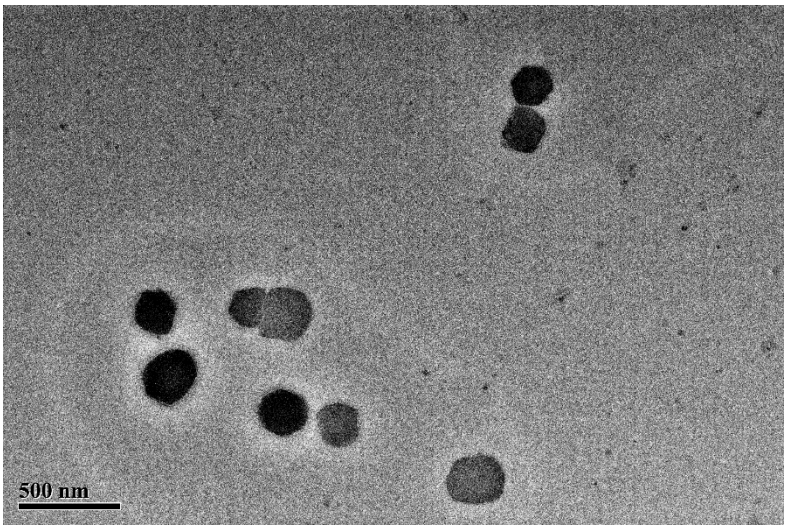

Fig. S62 TEM images of PDI/MLGG-6C⊂CB[8] assembly (the molar ratios of PDI, MLGG-6C, and CB[8] were 1:2:2).

20.ROS CLSM images of PDI/MLGG-6C⊂CB[8] assembly

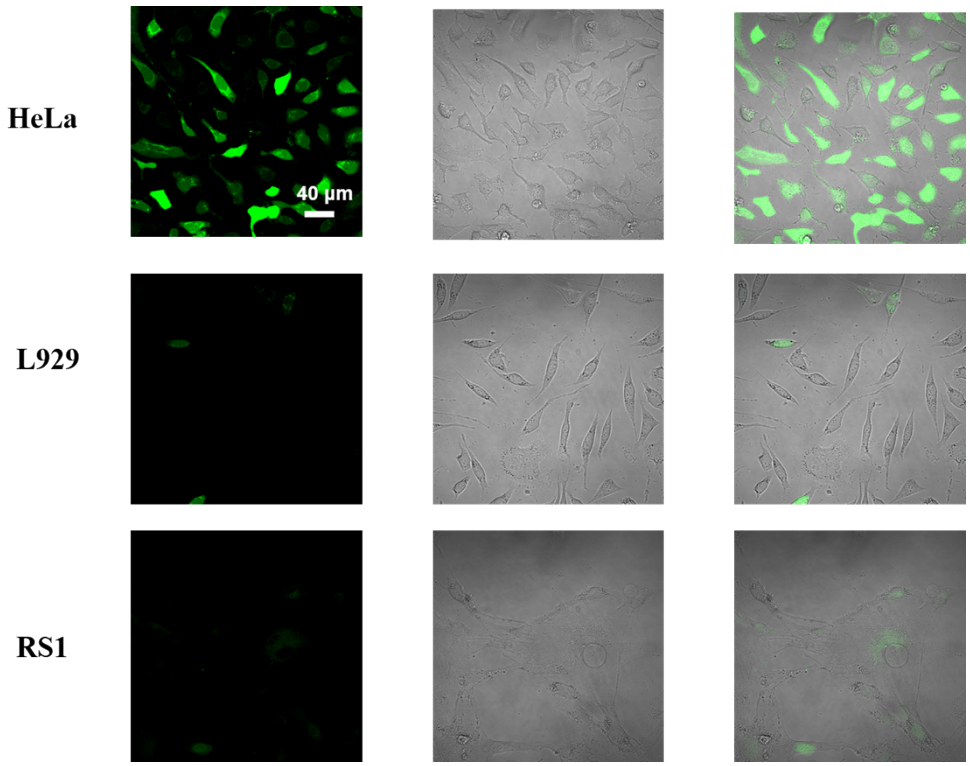

Fig. S63 ROS CLSM images of HeLa, L929 and RS1 cells.

21. CLSM images of PDI/MLGG-6C⊂CB[8] assembly

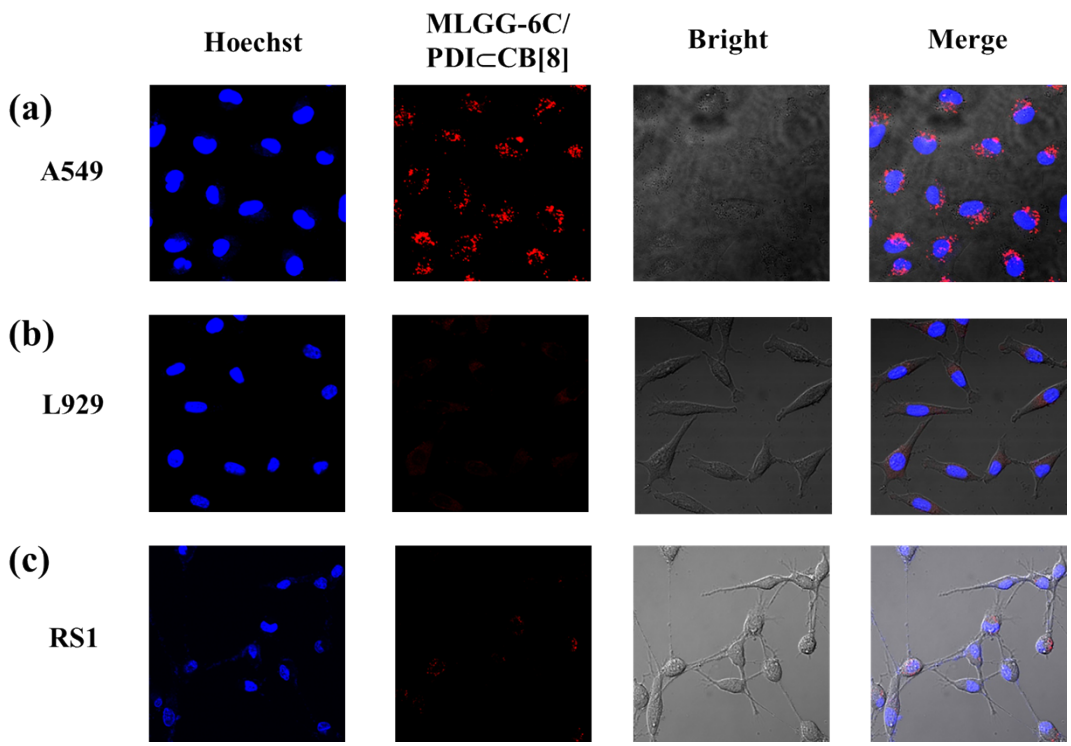

Fig. S64 CLSM images of (a) A549 cells, (b) L929 cells, and (c) RS1 cells treated with PDI/MLGG-6C⊂CB[8] assembly (PDI= 30 μM).

22. Pearson correlation coefficient of PDI/MLGG-6C⊂CB[8] assembly

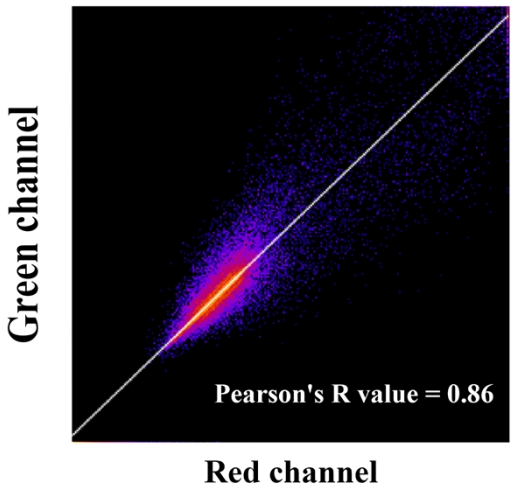

Fig. S65 Pearson correlation coefficient of PDI/MLGG-6C⊂CB[8] assembly.

23. Cell viability of MLGG-6C and MLGG-6C⊂CB[8]

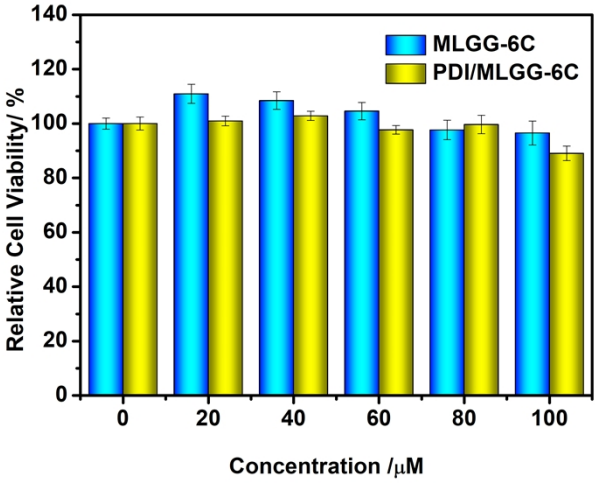

Fig. S66 Cell viability of HeLa cells treated with MLGG-6C, PDI/MLGG-6C.

24. ROS CLSM images and cell viability at elevated ROS level

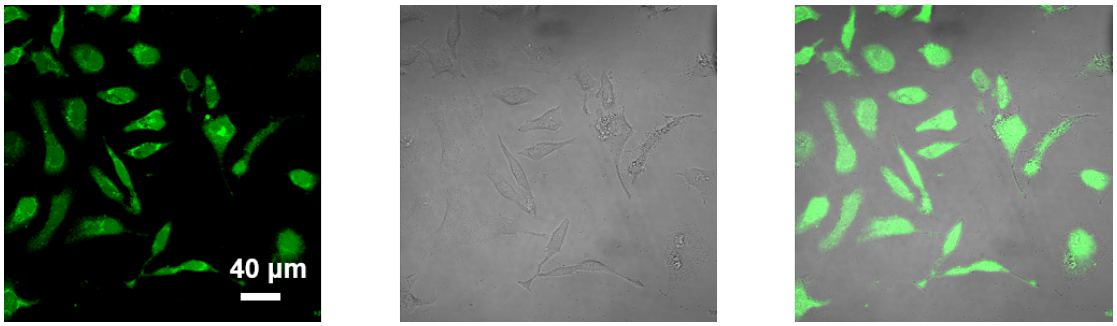

Fig. S67 CLSM images of HeLa cells treated with 100 μM H_2O_2.

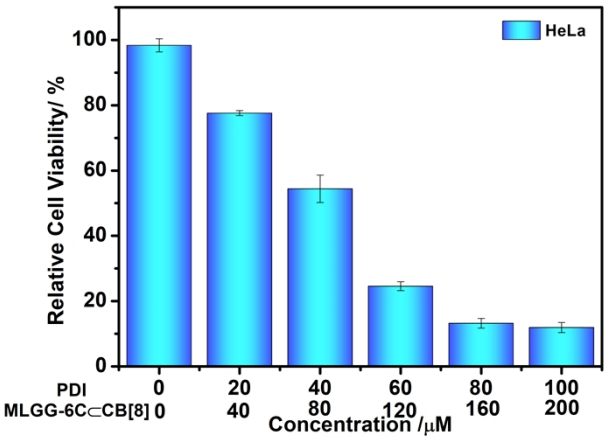

Fig. S68 Cell viability of HeLa cells treated with 100 μM H_2O_2 and then treated with PDI/MLGG-6C⊂CB[8] assembly.

25. ROS CLSM images and cell viability in normal cells

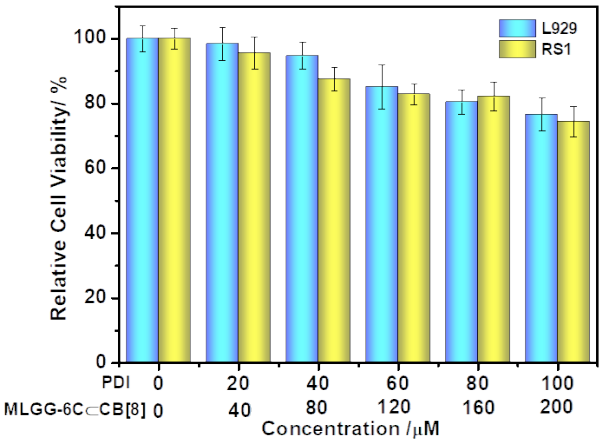

Fig. S69 In vitro cell viability of L929 and RS1 cells after being treated with PDI/MLGG-6C⊂CB[8] assembly at different concentrations for 24 h. The concentrations were calculated based on PDI.

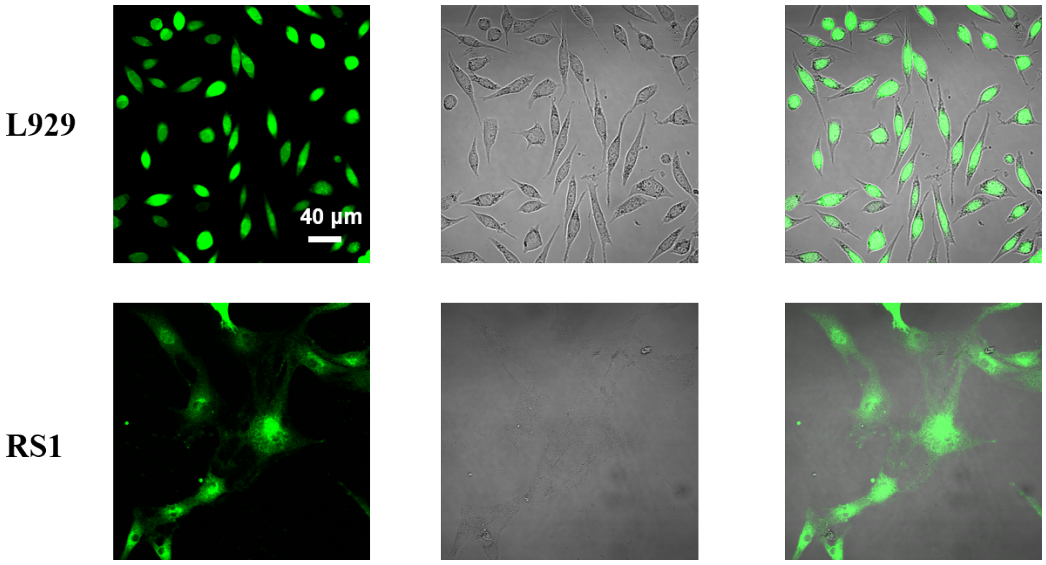

Fig. S70 ROS CLSM images of L929 and RS1 cells treated with 100 μM H_2O_2.

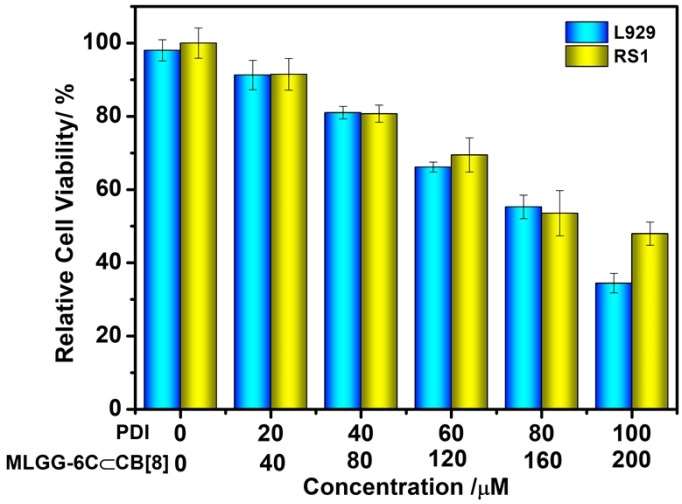

Fig. S71 Cell viability of L929 and RS1 cells treated with 100 μM H_2O_2 and then with PDI/MLGG-6C⊂CB[8] assembly.

References

S1 P. Thordarson, *Chem. Soc. Rev.*, 2011, **40**, 1305-1323.

S2 F. Biedermann, E. Elmalem, I. Ghosh, W. M. Nau, O. A. Scherman, *Angew. Chem. Int. Ed.*, **2012**, *51*, 7739-7743.

S3 S.-W. Tam-Chang, J. Helbley, I. K. Iverson, *Langmuir,* **2008**, *24*, 2133-2139.

S4 Y.-M. Zhang, Z. Wang, L. Chen, H.-B. Song and Y. Liu, *J. Phys. Chem. B*, 2014, **118**, 2433-2441.